

Magnetic Fe₃O₄ nanoparticles loaded papaya (*Carica papaya* L.) seed powder as an effective and recyclable adsorbent material for the separation of anionic azo dye (Congo Red) from liquid phase: Evaluation of adsorption properties



Venkata Subbaiah Munagapati^a, Hsin-Yu Wen^b, Anjani R.K. Gollakota^c, Jet-Chau Wen^{a,c,*}, Chi-Min Shu^{c,*}, Kun-Yi Andrew Lin^d, Zhong Tian^e, Jhy-Horng Wen^f, Guda Mallikarjuna Reddy^g, Grigory V. Zyryanov^{g,h}

^a Research Centre for Soil & Water Resources and Natural Disaster Prevention (SWAN), National Yunlin University of Science and Technology, Douliou, Yunlin 64002, Taiwan, ROC

^b Department of Pathology, West China Hospital, Sichuan University, Chengdu 610041, PR China

^c Department of Safety, Health, and Environmental Engineering, National Yunlin University of Science and Technology, Douliou, Yunlin 64002, Taiwan, ROC

^d Department of Environmental Engineering, National Chung Hsing University, 250 Kuo-Kuang Road, Taichung, Taiwan, ROC

^e State Key Laboratory of Hydraulics and Mountain River Engineering, Sichuan University, Chengdu, PR China

^f Department of Electrical Engineering, Tunghai University, Taichung 40704, Taiwan, ROC

^g Chemical Engineering Institute, Ural Federal University, 620002 Yekaterinburg, Russian Federation

^h Ural Division of the Russian Academy of Sciences, I. Ya. Postovskiy Institute of Organic Synthesis, 22 S. Kovalevskoy Street, Yekaterinburg, Russian Federation

ARTICLE INFO

Article history:

Received 26 September 2021

Revised 22 November 2021

Accepted 30 November 2021

Available online 3 December 2021

Keywords:

Adsorption mechanism

Fe₃O₄-PSP

Magnetic separation

Congo red

Regeneration

ABSTRACT

Magnetic adsorbents have recently gotten a lot of attention because of their eco-friendliness, ease of separation, and inexpensive cost. In this work, a new magnetic Fe₃O₄ loaded papaya seed powder (Fe₃O₄-PSP) was successfully synthesized and utilized as a biosorbent to eliminate Congo Red (CR) from the liquid phase. The prepared Fe₃O₄-PSP was characterized by BET, FE-SEM/EDX, VSM, XRD, pH_{PZC}, and FT-IR analysis. Batch tests were carried out to assess the influence of several adsorption factors like temperature (303–333 K), pH function (2.0–10.0), CR initial concentration (100–400 mg/L), Fe₃O₄-PSP mass (0.01–0.08 g/30 mL), and contact time (0–420 min). The pH_{PZC} of Fe₃O₄-PSP was computed at 5.4. Four kinetic models were used to analyze the kinetic data, and the most appropriate model with an *R*² value of 0.9991 was the pseudo-second-order. In accordance with the intra-particle diffusion model, the adsorption follows a three-step mechanism. The adsorption equilibrium data were examined using Dubinin-Radushkevich (D-R), Freundlich, Langmuir, and Temkin models and the adsorption data were well represented by the Langmuir isotherm (*R*² = 0.9962). The saturated adsorption efficiency of Fe₃O₄-PSP calculated from the Langmuir model was 216.9 mg/g at 303 K. The data was examined using error and regression coefficient functions, such as the χ^2 and SSE, to define the best-suitable isotherm and kinetic models. Hydrogen bonding and electrostatic interactions between CR and Fe₃O₄-PSP are responsible for the primary adsorption mechanism. The thermodynamic factors ΔS° (64.8 J/mol K), ΔG° (–1.1997 ~ 3.1439 kJ/mol for 303 ~ 333 K), and ΔH° (18.4 kJ/mol) revealed that the adsorption of CR onto Fe₃O₄-PSP was feasible, spontaneous, and endothermic. The saturation magnetization of Fe₃O₄-PSP was found to be 54.4 emu/g. An external magnetic field can regenerate and easily separate Fe₃O₄-PSP from an aqueous solution with no weight loss. According to the findings, Fe₃O₄-PSP is a potentially recyclable adsorbent for removing CR dye from contaminated water.

© 2021 Elsevier B.V. All rights reserved.

* Corresponding authors.

E-mail addresses: wenjic@yuntech.edu.tw (J.-C. Wen), shucm@yuntech.edu.tw (C.-M. Shu).

1. Introduction

The textile industries have a strong influence on the country's economy, but the dyeing and finishing processes from textile, leather, and dye industries create a significant amount of wastewater that pollutes the environment, endangers public health, and affects biodiversity [1]. One of the industries that emit significant

Nomenclature

| | | | |
|-----------------------------|--|----------------------|---|
| A_T | equilibrium binding constant | q_{e1}, q_{e2} | amount of dye adsorbed at equilibrium |
| b_T | Temkin constant | q_t | adsorption uptake at time t |
| C_o and C_e | initial and equilibrium CR solution concentrations | q_{max} | adsorption uptake |
| C_{Ae} | solid phase concentration at equilibrium | q_s | theoretical isotherm saturation uptake |
| C | intercept | R | universal gas constant (8.314 kJ/mol K) |
| k_1 and k_2 | PFO and PSO rate constants | SSE | sum of the squares of the error |
| K_c | distribution constant | t | time in min |
| K_f | Freundlich constant | T | temperature (K) |
| K_{id} | intra-particle diffusion rate constant | V | volume of CR solution (L) |
| K_L | Langmuir constant | | |
| K | constant related to sorption energy | <i>Greek letters</i> | |
| M | wight of Fe_3O_4 -PSP | ΔG^o | Gibbs free energy change |
| n | Freundlich exponent | ΔS^o | change in entropy |
| $1/n$ | heterogeneity factor | ΔH^o | change in enthalpy |
| N | number of adsorption tests | α | initial adsorption rate |
| q_e | amount of CR adsorbed | β | desorption constant |
| $q_{e,exp}$ and $q_{e,cal}$ | experimental and calculated adsorption capacities | ε | Polanyi potential |
| | | χ^2 | Chi-square |

amounts of wastewater owing to the use of water in manufacturing activities, such as washing, bleaching, dyeing, etc., is the textile industry [2]. Because textile factories discharge wastewater into fresh and groundwater bodies without appropriate treatment, water quality degrades and the quality of drinking water and agriculture suffers [1]. Due to its easy visibility and toxicity, the low concentration of dye in water is unwanted and unacceptable [1,3]. A large quantity of various kinds of dyes enters the waterways, where they affect human health. These environmental contaminants include carcinogens, which can cause cancer; toxicants, which can damage the central nervous system; and mutagens, which can cause birth defects [4]. The use of a dye in marine water also threatens aquatic life, resulting in a rise in biochemical oxygen demand (BOD) and chemical oxygen demand (COD). These additional demands lead to a reduced amount of light entering the water, which has a negative impact on plant growth and photosynthesis reactions [5]. So from an environmental standpoint, it is a major problem to remove harmful anionic or cationic dyes from industrial effluents before releasing them into water bodies.

Congo red is a highly colored synthetic azo dye. Research has shown that the main cause of an allergic response is caused by this dye's influence on a live organism. The formation of carcinogenic compounds, which serve as skin, ocular, and gastrointestinal irritants, is accelerated as dye degrades [6]. Also, respiratory and sleepiness issues are developed. As a result, red blood cells are raised. Because Congo red is poisonous in wastewater, it has been acknowledged that there is a significant issue with community health in the environment. While this dye is commonly used in the textile, biological stain, paper, printing, leather, and plastic industries for coloring their products [7]. This means that it must remove CR from wastewater effluents before combining them with uncontaminated natural water sources.

Conventional biological (e.g., aerobic/anaerobic degradation, microbial oxidation), chemical (e.g., advanced oxidation processes), and physical (e.g., coagulation, membrane filtration) techniques have been exploited for the treatment of dye-contaminated wastewater [8]. However, many of these methods cannot be used on a large scale due to high cost, less efficiency, high working cost, generation of harmful substances and intensive energy requirements [9]. Dyes, pigments, and other colorants in wastewater may be removed using adsorption. It has been shown to be the most effective of the different methods; it is simple and can be

adjusted quickly, there are no hazardous by-products produced, and it is also renewable [10].

Recently, agricultural waste has gained attention as a cost-effective adsorbent due to its abundance and affordability. In literature, a large category of adsorbents such as farming and forestry by-products, like cucumber peel [11], barberry stem [12], cabbage waste powder [13], *salix babylonica* [14], watermelon rind [15], *moringa oleifera* seed [16], sugar cane bagasse [17], and others have been successfully used for the removal of dyes from the liquid phase. Among all the fruits, papaya is the most eaten fruit worldwide, and 15.36% of the tropical fruit crop is made up of papaya [18]. In this fruit, nearly 15–20% of the wet weight comprises the seeds, which are not usually consumed. Therefore, the overall waste biomass produced would be roughly 2380 tons. This is again a type of organic pollution [19]. High-added-value chemicals found in papaya seeds contribute to some of the benefits of this fruit. A number of seed proteins (24.31 g), oils (25.32 g), total carbohydrates (32.54 g), total dietary fiber (17.11 g), ash (0.09 g), and volatile oil (0.09 g) are present in the seeds [20]. The research showed that papaya seeds are used in medicine and are also effective for removing various colors, metals, and turbidity from wastewater [21]. From an environmental and economic standpoint, using papaya seeds as an adsorbent is extremely intriguing since it is an agricultural leftover at a cheap cost. However, it is necessary to take into consideration the limits of utilizing waste from agriculture to be adsorbents, like possible leaching of plant soluble components into treated water, lower adsorption efficiency due to diffusion restrictions, lower specific surface area, and difficulties removing after the adsorption process is completed [22]. Particular emphasis was given to the use of magnetic adsorbents to overcome these constraints.

Besides, recent research trends have focused on introducing magnetic properties as the magnetic core within composite adsorbents to achieve the effective separation and accessible collection of adsorbents from the liquid phase by an external magnetic field. Magnetic separation has several advantages. One of them is that it is extremely simple and efficient, requiring minimal work and expense. Magnetite iron oxide nanoparticles (Fe_3O_4) are incorporated into agricultural waste, which improves the surface area and reactivity while reducing intra-particle diffusion. Adsorption capacity and reusability are also enhanced. Recently, magnetic Fe_3O_4 nanoparticle loaded adsorbents such as *solanum tuberosum* peel [23], amine modified hydrochar [24], activated carbon [25],

Fe₃O₄ loaded chitin [26], wheat straw [27], biochar [28], pomegranate leaves [29], etc. have been utilized to remove dyes from the liquid phase effectively.

We prepared Fe₃O₄-PSP as a highly proficient biosorbent combining easy phase separation and high selective sorption capability to eliminate CR dye in the present study. Characterization of the Fe₃O₄-PSP adsorbent is analyzed through the point of zero charge (pH_{PZC}), fourier transform infrared (FTIR) spectroscopy, Brunauer-Emmett-Teller (BET), field emission-scanning electron microscopy/energy-dispersive X-ray spectroscopy (FE-SEM/EDX), X-ray diffraction (XRD), and vibrating sample magnetometer (VSM). Furthermore, various factors such as influence of pH, Fe₃O₄-PSP mass, temperature, absorptive time, and initial CR concentration were examined. Moreover, the equilibrium isotherms, kinetics, and thermodynamics of the adsorption process of the CR on the prepared Fe₃O₄-PSP were studied. Also, the adsorption-desorption of CR dye was carried out for several cycles to establish the reusability potential of the Fe₃O₄-PSP.

2. Materials and methods

2.1. Materials

Sodium hydroxide (NaOH), hydrochloric acid (HCl), diethylenetriamine (NH₂CH₂CH₂)₂NH, ferric chloride hexahydrate (FeCl₃·6H₂O), ferrous sulfate heptahydrate (FeSO₄·7H₂O), and Congo Red (molecular weight; 696.66 g/mol, linear formula; C₃₂H₂₂N₆Na₂O₆·S₂, dye content; ≥35%, λ_{max}: 497 nm) were procured from Sigma Aldrich Company (USA) and was utilized as received without additional purification. Distilled water (DW) was used to make all of the solutions. To make stock and diluted dye solutions for subsequent investigations, a properly weighed quantity of the CR was dissolved in DW. Fig. 1 illustrates the molecular structure of CR.

2.2. Preparation of Fe₃O₄-PSP

Fruits of the papaya (*Carica papaya* L.) were purchased at a nearby market (Douliou, Taiwan). The seeds were carefully extracted from fresh papaya fruit and rinsed (many times) with DW to remove dust and other impurities. The seeds were boiled for 8 h to get rid of transparent gelatinous aril then washed with DW. The cleaned seed was then oven-dried at 343 K for 48 h to remove all moisture content. Following that, the dried seeds were pulverized into fine particles. The pulverized seed powder was kept in a tight container in a cool, dry area until further treatment. The obtained powder was labeled as PSP.

Fe₃O₄ loaded PSP was generated from chemical coprecipitation. Firstly, 6.0 g of FeCl₃·6H₂O and 11.75 g of FeSO₄·7H₂O were put into a beaker containing 600 mL of DW, with constant stirring at 343 K for 1 h. After that, 20 g of the PSP was added with continuous stirring for 30 min, followed by 0.5 M NaOH solution to adjust to pH 11.0. The color of the reaction mixture was changed from dark brown to black. The cooled solution was tested and found to be attracted to a magnet indicating the formation of a magnetic com-

posite adsorbent, after which it was centrifuged for 15 min at 8000 rpm. The residue was washed with excess distilled water until pH 7.0, centrifuged again, and dried for 5 h in an oven at 353 K. The dried composite was then pulverized to a fine powder and passed through a 0.35 mm mesh sieve to obtain the Fe₃O₄ loaded PSP nanocomposite, designated as magnetic Fe₃O₄-PSP.

2.3. Instrumentation

The surface functional groups of the materials (PSP, Fe₃O₄-PSP, and CR-loaded Fe₃O₄-PSP) were determined using Nicolet IS10 Thermo Fisher Scientific FTIR spectroscopy in the region of 400–4000 cm⁻¹. 10 mg of material was combined with 100 mg of KBr to make a pellet for IR spectral analysis. A pure KBr pellet was used to determine the background absorbance. The surface morphological and elemental composition of samples were performed using FE-SEM using a JEOL JSM-7610F Plus model equipped with an EDX analyzer. The surface of the samples was gold-coated before the analysis. The surface area and pore size distribution were carried out by the BET (Brunauer-Emmett-Teller) and BJH (Barrett-Joyner-Halenda) method through N₂ adsorption/desorption analysis using the ASAP 2060 (Micrometrics) analyzer at 77 K. The materials were degassed at 473 K for 2 h before examination. The phase and structural characteristics of the samples (PSP and Fe₃O₄-PSP) were characterized by X-ray diffraction (XRD, Bruker Advanced-D825A) with Cu-K_α (λ = 1.54060 Å) radiation in the 2θ range of 2–80°. The magnetic behavior of the Fe₃O₄-PSP was analyzed by a Vibrating Sample Magnetometer (VSM-7400, Lakeshore, USA) with the range of magnetic field between –20000 and +20000 Oe at 298 K. The solid addition method [30] was used to estimate the Fe₃O₄-PSP's point of zero charge (pH_{PZC}). In brief, 30 mL of KNO₃ (0.01 M) was put into 50 mL glass vials, and the initial pH (pH_i) was maintained between 2.0 and 10.0 by adding 0.1 M HCl/NaOH solutions. At each pH was individually mixed with the pre-weighed Fe₃O₄-PSP (0.05 g). The resultant solutions were agitated at 200 rpm for 24 h at room temperature, and the pH_f (final pH) was determined using a pH-meter (Mettler Toledo S20-K, USA). pH_i was plotted against ΔpH, which was derived as the variance between pH_i and pH_f values. The horizontal line intersection point (X axis) in the diagram is ΔpH = 0 is the pH_{PZC} value.

2.4. Performances of adsorption

The batch adsorption tests were performed on a temperature controlled thermostatic reciprocating shaker with a constant shaking speed of 200 rpm. To investigate the pH solution, 50 mg of Fe₃O₄-PSP was combined with 30 mL of CR solution (100 mg/L) at 303 K for 180 min at the indicated pH range (2.0–10.0). 0.1 M NaOH/HCl was used to adjust the pH of the initial solution from 2.0 to 10.0. The kinetics test was done by combining 0.05 g Fe₃O₄-PSP with 30 mL of CR solution (pH 5.0, 100–400 mg/L), followed by a sorption procedure at 303 K for time intervals of 0 to 420 min. The isotherm evaluation consisted of an adsorption test at pH 5.0 with various initial concentrations of CR solutions (100–1000 mg/L), with the adsorption condition being the same as the pH effect. Similar experimental circumstances were employed to perform adsorption at several temperatures (303–333 K) for the thermodynamics study. The samples were extracted at certain time intervals after the adsorption process was finished, and the sorbent was separated by centrifugation at 8000 rpm for 15 min. A UV-Vis (Ultraviolet-Visible) spectrophotometer set to 497 nm was used to determine the concentration of residual CR in the solution. The q_e is the adsorption capability of CR onto

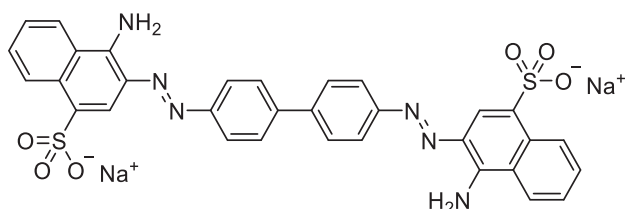


Fig. 1. Chemical structure of CR.

$\text{Fe}_3\text{O}_4\text{-PSP}$ (mg/g), and the percentage of CR removal (%) was determined from the following equations:

$$q_e = \frac{[C_o - C_e]V}{M} \quad (1)$$

$$R\% = \frac{C_o - C_e}{C_o} \times 100 \quad (2)$$

2.5. Desorption and regeneration studies

The regeneration of the utilized biosorbent was explored in order to assess the practical uses and commercial feasibility of the adsorption process. The experiments for CR desorption efficiency from $\text{Fe}_3\text{O}_4\text{-PSP}$ were carried out by using different eluents. Initially, the adsorption process was carried out with a known amount of $\text{Fe}_3\text{O}_4\text{-PSP}$ to treat 30 mL of dye concentration of 100 mg/L for 180 min. The loaded biosorbents were then separated from the adsorbate solution and agitated with the eluents for the desorption experiment at the same reaction time. After desorption, the mixture was centrifuged, and the concentrations of CR desorbed in the solutions were determined. The desorption percentage of CR from $\text{Fe}_3\text{O}_4\text{-PSP}$ adsorbent was calculated from the following equation:

$$\text{Desorption (\%)} = \frac{\text{Amount of CR desorbed}}{\text{Amount of CR adsorbed}} \times 100 \quad (3)$$

The aforementioned procedure was performed using the same adsorbent and experimental conditions for five consecutive adsorption/desorption experiments.

2.6. Error function analysis

One of the most frequently used regression procedures for fitting a prediction model to experimental data values is linear regression. To verify the best-suited isotherm for the adsorption system, as well as the intrinsic bias arising from the linear transformation, a variety of mathematical error functions may be used [31]. The isotherms and kinetic models in this study were validated using the non-linear χ^2 and the SSE error functions, as follows:

$$\chi^2 = \sum_{i=1}^n \left(\frac{(q_{e,\text{exp}} - q_{e,\text{cal}})^2}{q_{e,\text{cal}}} \right) \quad (4)$$

$$\text{SSE} = \sqrt{\sum \frac{q_{e,\text{exp}} - q_{e,\text{cal}}}{N}} \quad (5)$$

A decrease in errors indicates that the data produced by the model is comparable to the experimental result. Based on the greater values of the linear regression correlation coefficient and the lower values of χ^2 and SSE, the best-suitable model was verified.

3. Results and discussion

3.1. Characterization

The FT-IR spectra of PSP, $\text{Fe}_3\text{O}_4\text{-PSP}$, and CR-adsorbed $\text{Fe}_3\text{O}_4\text{-PSP}$ are displayed in Fig. 2. FT-IR spectrum of PSP exhibits adsorption bands at 3435, 2893, 1638, 1412, 1324, 1017, and 778 cm^{-1} (Fig. 2(a)). The peak at 3439 cm^{-1} was ascribed to stretching vibrations of the hydroxyl group present in the PSP. The band located at 2893 cm^{-1} indicates the C-H stretching vibration in CH and CH_2 . The band at 1638 cm^{-1} could be assigned to the -C=O stretching vibration of the carbonyl group. The adsorption bands at 1412 and 1324 cm^{-1} could be attributed to the -C-O group. The peak

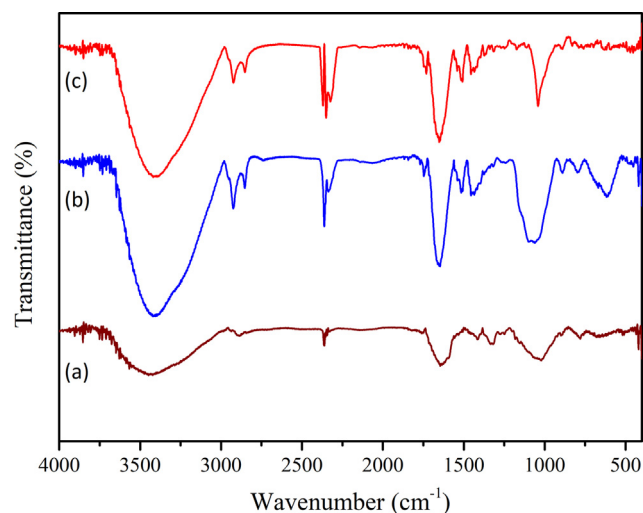


Fig. 2. FTIR spectral analysis of (a) PSP, (b) $\text{Fe}_3\text{O}_4\text{-PSP}$, and (c) CR-loaded $\text{Fe}_3\text{O}_4\text{-PSP}$.

at 1017 cm^{-1} was assigned to stretching vibrations of the C-O group. The presence of a band at 778 cm^{-1} is ascribed to C-H in out-of-plane bending vibrations. The FTIR spectrum of $\text{Fe}_3\text{O}_4\text{-PSP}$ shows the following adsorption bands at 3416, 2921, 2850, 1747, 1642, 1514, 1452, 1058, 887, 792, and 608 cm^{-1} . Compared with the PSP and $\text{Fe}_3\text{O}_4\text{-PSP}$, some peaks are slightly shifted, and some new peaks (2921, 1747, 1512, 887, and 608 cm^{-1}) appear (Fig. 2 (b)). The band at 3435 cm^{-1} is due to the overlapping of the stretching bands of primary amine and -OH groups in the surface of $\text{Fe}_3\text{O}_4\text{-PSP}$. The bands at 2921 and 2851 cm^{-1} are ascribed to the asymmetric and symmetric stretching vibration of C-H. The new band at 1747 cm^{-1} can be assigned to the carboxylate group bonded onto the surface of $\text{Fe}_3\text{O}_4\text{-PSP}$. The bands at 1642 and 1452 cm^{-1} were attributed to the symmetric and asymmetric stretching vibrations of carboxylate groups, respectively. The peak at 1512 cm^{-1} that corresponds to either the deformation of -CH_2 or the bending of -NH_2 . The peak at 1058 cm^{-1} was assigned for stretching vibrations of C-O in -C-OH . The band positions at 887 and 792 cm^{-1} were attributed to the out-of-plane bending vibration of C-OH. The characteristic absorption band at 608 cm^{-1} corresponds to the stretching vibration of Fe-O in the spectrum of $\text{Fe}_3\text{O}_4\text{-PSP}$, demonstrating that the Fe_3O_4 particles were successfully loaded on the PSP surface. The FTIR spectrum of $\text{Fe}_3\text{O}_4\text{-PSP}$ after adsorption of CR (Fig. 2(c)) displays the same bands in the spectrum of $\text{Fe}_3\text{O}_4\text{-PSP}$ (Fig. 2(b)) with a slight shifting of some peaks (3416, 1747, 1514, and 1058 cm^{-1} to 3406, 1730, 1507, and 1038 cm^{-1}) and two peaks are disappeared (794 and 608 cm^{-1}), indicating that the functional groups of $\text{Fe}_3\text{O}_4\text{-PSP}$ were successfully involved in the CR dye adsorption process.

The surface morphological structure and elemental composition of PSP, $\text{Fe}_3\text{O}_4\text{-PSP}$, and $\text{Fe}_3\text{O}_4\text{-PSP}$ after CR sorption were examined by FESEM-EDX analysis. Fig. 3(a-c) illustrates the obtained findings of the SEM pictures and EDX analysis for PSP, $\text{Fe}_3\text{O}_4\text{-PSP}$, and $\text{Fe}_3\text{O}_4\text{-PSP}$ after adsorption of CR dye, respectively. As seen in Fig. 3(a), the surface morphology of PSP appears as an irregular and heterogeneous surface. The EDX analysis shows that the PSP surface contains mainly the elements C, O, Mg, S, Cl, K, and Ca. The surface morphology of PSP after loading Fe_3O_4 (Fig. 3(b)) into its surface was changed to be rougher, more irregular, with the existence of several sizes of pores and cavities. Surface roughness plays an essential role in dye ion binding because it increases the contact area, facilitating dye sorption on the surface. The EDX analysis corresponding to $\text{Fe}_3\text{O}_4\text{-PSP}$ reveals the presence of C, O, S, and Fe. The existence of a Fe peak in the EDX spectrum confirms that

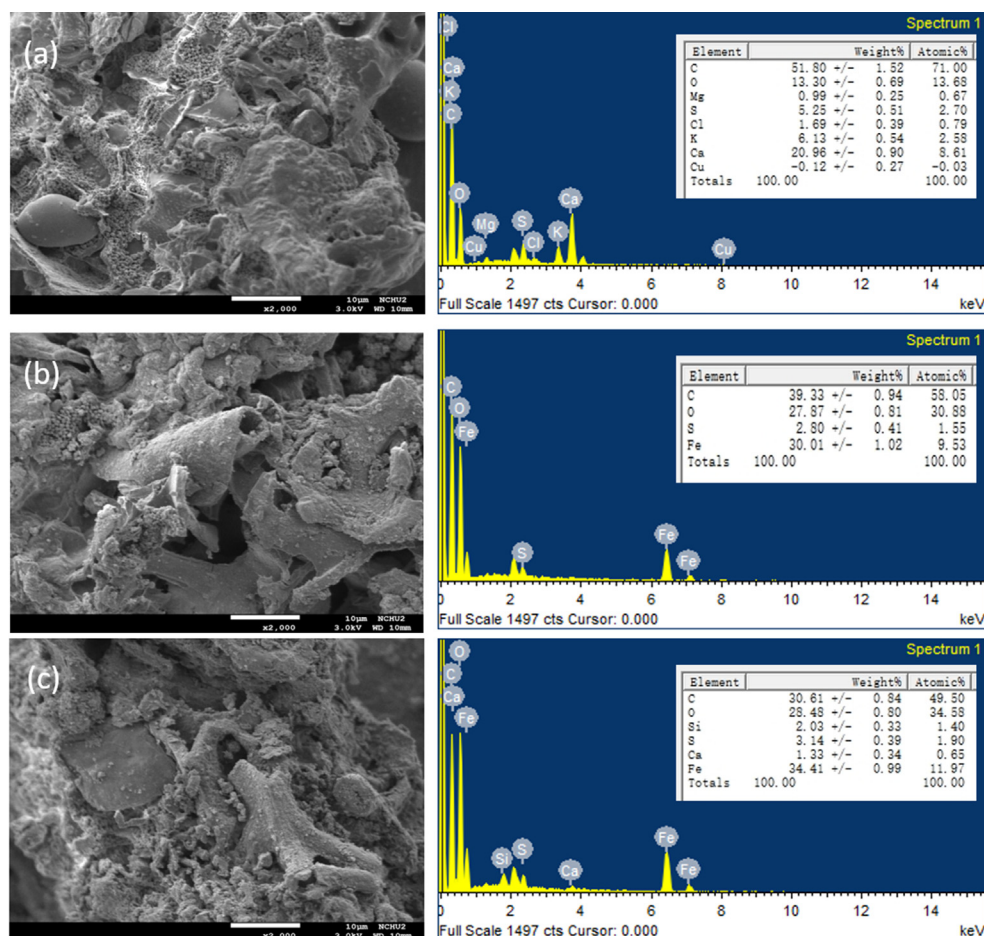


Fig. 3. SEM-EDX analysis of (a) PSP, (b) Fe₃O₄-PSP, and (c) CR-loaded Fe₃O₄-PSP.

the Fe₃O₄ particles were loaded successfully onto the PSP surface. The Fe₃O₄-PSP after CR adsorption was considerably smoother as a result of the loading of CR dye molecules on its surface (Fig. 3 (c)). The EDX analysis shows that the S element belongs to CR dye and reconfirmed the CR dye adsorption by Fe₃O₄-PSP surface.

One of the key factors to control adsorption efficiency is the BET analysis. The greater specific surface area in BET analysis indicates that more empty sites on the adsorbent surface are available. Fig. 4 (a,c) illustrates the N₂ adsorption/desorption isotherms of PSP and Fe₃O₄-PSP, which can be categorized as type-IV isotherm with an H₃-type hysteresis loop based on IUPAC classification, indicating that the mesoporous nature of the surface [32]. The textural parameters of the PSP and Fe₃O₄-PSP are listed in Table 1, which shows the pore volume and pore diameter values of Fe₃O₄-PSP were greater compared to the PSP. Similarly, the BET surface area of Fe₃O₄-PSP increased approximately ~ 8.6 times by loading Fe₃O₄ nanoparticles into the surface of PSP, which made it more favorable for the adsorption process. Furthermore, the pore size distribution of both PSP and Fe₃O₄-PSP (Fig. 4(b,d)) was determined using the BJH method. According to the IUPAC, pore sizes are categorized based on the pore diameter (D), i.e., D > 50.0 nm (macropores), 2.0 < D < 50.0 nm (mesopores), and D < 2.0 nm (micropores) [33]. In the current study, the peaks of pore size distribution were found to be at 1.572 and 2.214 nm for PSP and Fe₃O₄-PSP, respectively. These findings indicate that Fe₃O₄-PSP has a higher surface area and mesopores and may be used as a viable adsorbent for removing contaminants from wastewater.

The XRD spectrum of the PSP and Fe₃O₄-PSP are demonstrated in Fig. 5. The XRD pattern of PSP (Fig. 5(a)) has shown two

diffraction peaks at 20.8 and 43.2°, which are assigned to the reflection from (002) and (101) planes, respectively [34]. The broader peak of PSP appearing at 20.8° was attributed to better layer alignment and uniformity of the crystal structure and a weak peak appear at 43.2° was an indication of an amorphous structure [35]. The prepared Fe₃O₄-PSP (Fig. 5(b)) exhibited several characteristic peaks appearing at 2θ = 21.2, 30.2, 35.9, 43.2, 53.1, 57.4, and 63.2° ascribed to the (111), (220), (311), (400), (422), (511), and (440) reflection planes respectively were characteristic of face-concentrated cubic magnetite Fe₃O₄ (JCPDS No: 19-0629) [24]. The Fe₃O₄-PSP findings indicated that Fe₃O₄ nanoparticles were effectively formed on the surface of PSP.

The magnetic behavior of Fe₃O₄-PSP had been examined using VSM at room temperature. The VSM hysteresis loop of the Fe₃O₄-PSP sample was represented in Fig. 6. The S-shaped curve with nearly zero hystereses showed the superparamagnetic behavior of the Fe₃O₄-PSP [36]. The saturation magnetization value of Fe₃O₄-PSP is 54.4 emu/g, indicating that the adsorbent could be readily separated from the liquid phase using a strong external magnet. Fig. 6 (inset) shows that the Fe₃O₄-PSP can be collected from a liquid solution under an external magnetic field. This property is essentially significant for the convenient recycling of the Fe₃O₄-PSP.

3.2. Influence of pH

The pH has a significant impact on a number of important variables, including surface charge at the biosorbent's surface, the magnitude of ionization and dissociation of functional groups.

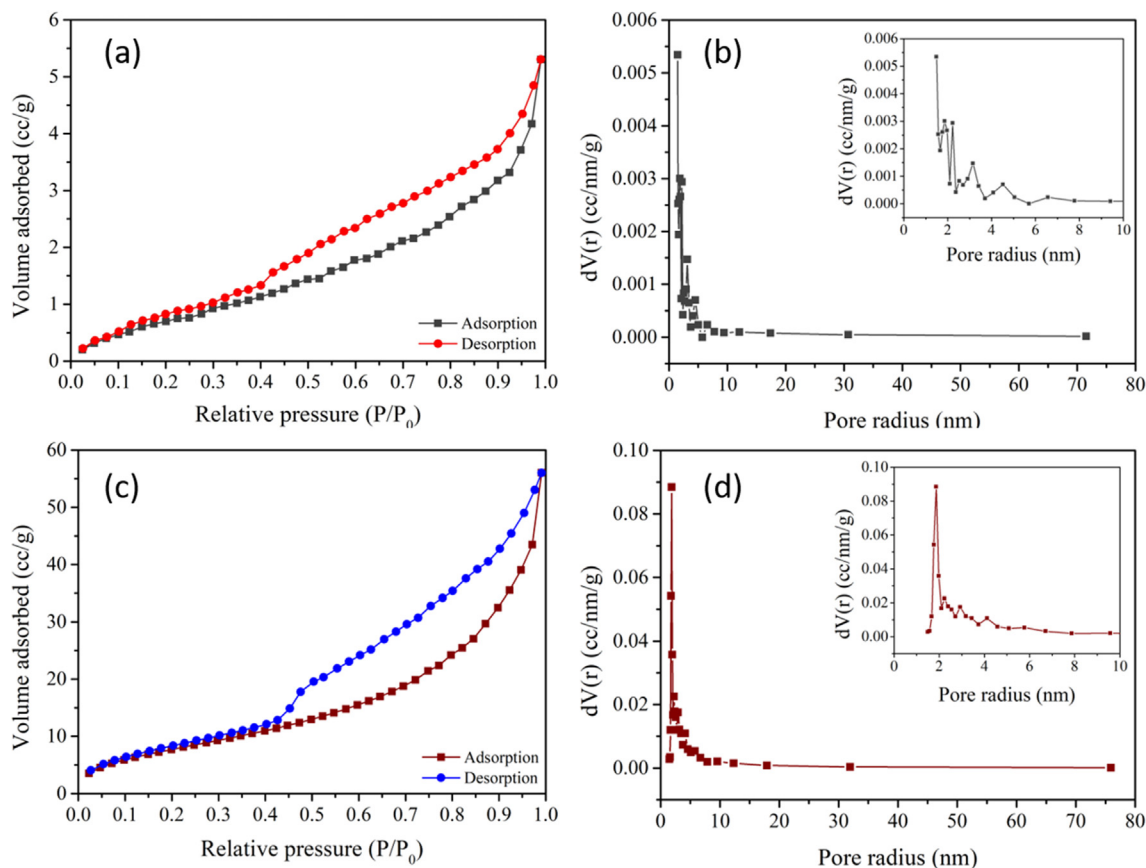


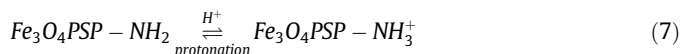
Fig. 4. BET N₂ adsorption-desorption isotherms of (a) PSP and (c) Fe₃O₄-PSP, and the pore size distribution plots of (b) PSP and (d) Fe₃O₄-PSP.

Table 1
Characteristics of PSP and Fe₃O₄-PSP.

| Adsorbent | BET surface area (m ² /g) | Pore volume(cc/g) | Pore radius(nm) |
|-------------------------------------|--------------------------------------|-------------------|-----------------|
| PSP | 3.67 | 0.0036 | 1.572 |
| Fe ₃ O ₄ -PSP | 30.54 | 0.0946 | 2.214 |

capacity showed a dramatic increase when the solution pH rose from 2.0 to 5.0; then, the sorption capacity significantly reduced when further increased the pH. The maximal adsorption capacity of CR adsorbed on the Fe₃O₄-PSP surface was 85.6 mg/g at pH 5.0. The pH impact may also be clarified by the zero-charge point of the adsorbent (pH_{PZC}). When the pH value is lower than the pH_{PZC}, the positive charge appears on the surface of the biosorbent. Conversely, when the pH value is greater than the pH_{PZC}, their surfaces are charged negatively. The pH_{PZC} value obtained for Fe₃O₄-PSP was pH 5.4 (Fig. 7(b)), thus, indicative of the acidic nature of the Fe₃O₄-PSP surface. When raising the pH from 2.0 to 5.0, the adsorption capability obviously increases since the surface of Fe₃O₄-PSP will acquire a positive charge due to -OH, -NH₂, and -COOH groups protonated to form -OH₂⁺, -NH₃⁺, and -COOH₂⁺ groups, respectively, and an intense electrostatic attraction can be occurred between positively charged -OH₂⁺, -NH₃⁺, and -COOH₂⁺ groups and negatively charged -SO₃⁻ groups of the CR dye [37].

In an acidic medium, the positive sites can be achieved according to the reactions below:



In the aqueous system, sulphonate groups of the dye are dissociated and the dye becomes negative:

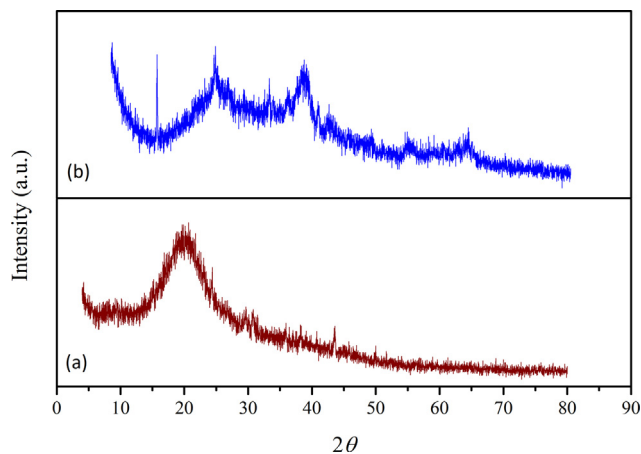


Fig. 5. XRD patterns of (a) PSP and (b) Fe₃O₄-PSP.

The influence of solution pH on the uptake of CR onto Fe₃O₄-PSP was identified at different pH levels (2.0–10.0) at the fixed values of the critical parameters (CR initial concentration 100 mg/L, mass 0.05 g, and contact time 180 min). From Fig. 7(a), the adsorption

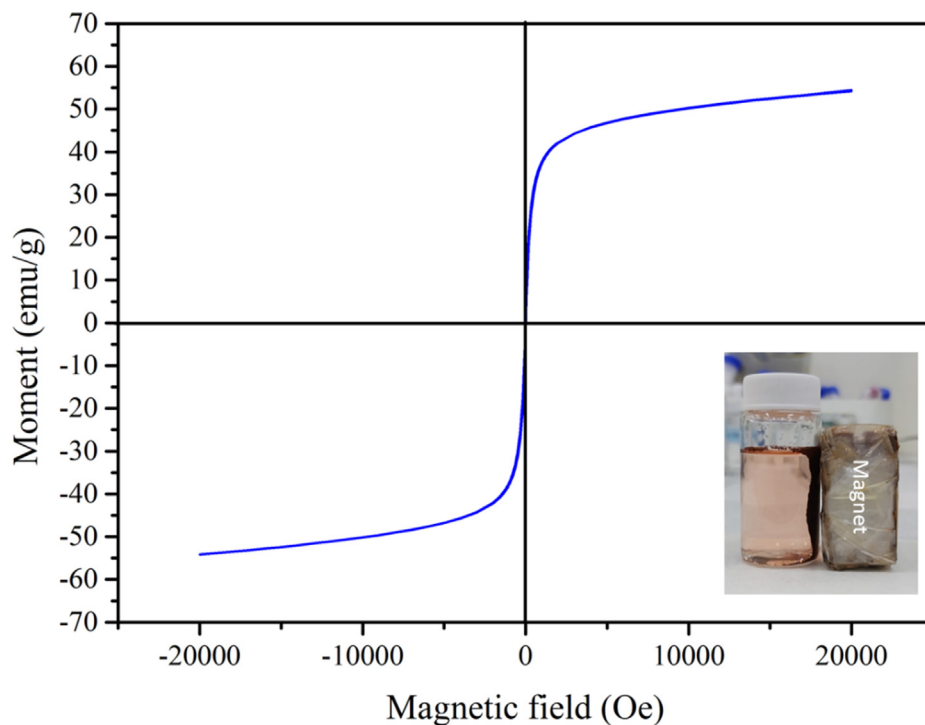


Fig. 6. Magnetic hysteresis loop of $\text{Fe}_3\text{O}_4\text{-PSP}$.

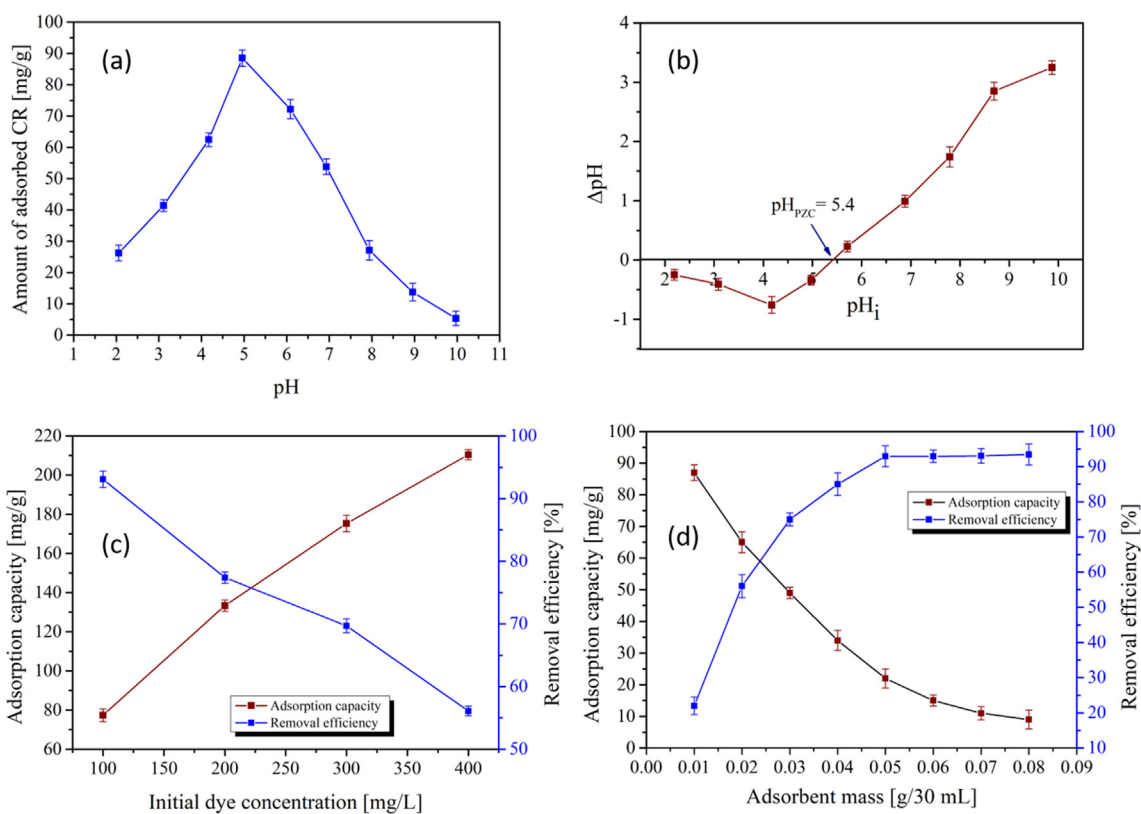


Fig. 7. Effect of (a) solution pH [adsorbent mass = 0.05 g; initial dye concentration = 100 mg/L; dye volume = 30 mL; shaking speed = 200 rpm; temperature = 303 K], (b) pH_{PZC} of $\text{Fe}_3\text{O}_4\text{-PSP}$ [electrolyte volume = 30 mL; adsorbent mass = 0.05 g; temperature = 303 K; shaking speed = 200 rpm], (c) initial dye concentration [adsorbent mass = 0.05 g; $\text{pH} = 5.0$; dye concentration = 100–400 mg/L; dye volume = 30 mL; shaking speed = 200 rpm; temperature = 303 K], and (d) adsorbent mass [initial dye concentration = 100 mg/L; dye volume = 30 mL; $\text{pH} = 5.0$; shaking speed = 200 rpm; time = 180 min; temperature = 303 K].



If the pH is over 5.0, the capacity of adsorption diminishes rapidly, owing to the increasing quantity of hydroxyl ions (OH^-) in the solution. Thus, for the surfaces of the adsorbent hydroxide ions with the CR anions complete, resulting in weak electrostatic interactions between the CR anions and the Fe_3O_4 -PSP [36]. For CR of MgFe_2O_4 - NH_2 and $\text{Zn-Fe}_2\text{O}_4$, a similar variation trend was observed between pH and maximum adsorption capacity [38,39]. Hence, pH = 5.0 for further adsorption tests was selected according to the aforementioned findings.

3.3. Influence of the initial CR concentration

The impact of initial CR concentration on Fe_3O_4 -PSP biosorption was studied by changing solution concentrations from 100 to 400 mg/L while keeping the other variables constant (temperature = 303 K, pH = 5.0, dye volume = 30 mL, and Fe_3O_4 -PSP mass = 0.05 g). The removal efficiency falls from 93.1 to 56.3% when the initial CR concentration rises from 100 to 400 mg/L, while the adsorption capability improves from 77.4 to 210.8 mg/g, as shown in Fig. 7(c). The initial dye concentration is a major driving force in overcoming the dye molecule mass transfer barrier between the solid and aqueous phases. The accessible adsorption sites of Fe_3O_4 -PSP are more than the number of dye molecules at lower starting dye concentrations. The adsorption ability of Fe_3O_4 -PSP for CR in this instance is determined by the number of accessible adsorption sites. The number of dye molecules is greater than the accessible adsorption sites of Fe_3O_4 -PSP at a higher initial dye concentration. Under these conditions, the concentration gradient's driving force increases as the dye concentration rises. To put it another way, the higher the dye concentration, the stronger the interaction between dye molecules and adsorbents, resulting in adsorbents with a larger adsorption capacity [40]. On the other hand, at higher concentrations, the removal efficiency dropped because the dye competed for the adsorbent's active binding sites, and there was insufficient free space to bind the dye molecules to the adsorbent surface [14]. At a CR concentration of 100 mg/L, the highest adsorption efficiency was found to be 93.1%, which was utilized in further adsorption tests.

3.4. Influence of Fe_3O_4 -PSP mass

The influence of Fe_3O_4 -PSP mass on the CR removal (100 mg/L) was measured in the range of 0.01 to 0.08 g/30 mL at pH 5.0 and contact duration of 180 min. As demonstrated in Fig. 7(d), raising the Fe_3O_4 -PSP mass from 0.01 to 0.08 g/30 mL raised the CR removal efficiency from 22 to 93.1%. The highest CR removal efficiency (93.1%) was achieved with 0.05 g/30 mL mass of Fe_3O_4 -PSP. This improved removal efficiency was ascribed to the combined effects of the increased surface area and the increased number of active sites available for adsorption, which enhanced dye adsorption [41]. However, no significant improvement in removal efficiency was found when the amount of Fe_3O_4 -PSP was increased because at too high a mass, the biosorbent particles clustered together to form clusters, which blocked certain adsorption sites. Furthermore, since the surface area did not increase substantially further, no additional improvement in removal efficiency was observed [42]. On the other hand, the adsorption ability (q_e) gradually decreased from 87.2 to 9.1 mg/g while increasing the mass from 0.01 to 0.08 g/30 mL (Fig. 7(d)). This phenomenon can be caused by the overlapped or aggregated adsorption sites, leading to a decrease in the total effective adsorption surface of the CR, thereby increasing the length of the diffusion path [43]. Therefore, 0.05 g/30 mL of Fe_3O_4 -PSP was chosen as an optimum biosorbent mass for the adsorptive removal of CR dye from a liquid phase.

3.5. Effect of contact time

Contact time tests are critical in describing adsorption rates and determining equilibrium times for dye adsorption. The impact of contact duration on the adsorption of CR by Fe_3O_4 -PSP was investigated at various starting dye solution concentrations ranging from 100 to 400 mg/L for up to 420 min, and the findings are shown in Fig. 8. The adsorption ability of Fe_3O_4 -PSP rose with increasing contact time at first, then progressively climbed to an equilibrium value in approximately 180 min for all dye concentrations, after which there was no significant change. At equilibrium, the amount of CR dye adsorbed was 77.5 mg/g (at 100 mg/L), 133.3 mg/g (at 200 mg/L), 175 mg/g (at 300 mg/L), and 210 mg/g (at 400 mg/L). Because of the greater interaction of adsorbate with empty adsorptive sites present on the top surface of the biosorbent during the initial stage of rapid adsorption, the dye adsorption rate is constant. Dye molecules filled the vacant sites following the equilibrium period, resulting in a repulsive force in the bulk phase between the Fe_3O_4 -PSP surface and CR [44]. Hence the equilibrium time was fixed at 180 min for further adsorption experiments.

3.6. Adsorption kinetic study

The adsorption kinetic study gave valuable information on the nature and the adsorption mechanism of the transition from the liquid phase to the solid phase. The adsorption of CR onto Fe_3O_4 -PSP was explored using three distinct kinetic models: PFO (pseudo-first-order), PSO (pseudo-second-order), and Elovich. The nonlinear forms of the PFO, PSO, and Elovich models may be described as the following equations:

$$q_t = q_{e1}(1 - \exp(-k_1t))q_t = \frac{q_{e2}^2 k_2 t}{1 + q_{e2} k_2 t} \quad (11)$$

$$q_t = \frac{1}{\beta} \ln(1 + \alpha\beta t) \quad (12)$$

Fig. 9 depicts the fitting of the kinetic models to the experimental data, while Table 2 contains the values of the fit parameters. The PSO kinetic model values better describe the adsorption kinetics of CR onto Fe_3O_4 -PSP than the PFO and Elovich model at all initial concentrations because of the high R^2 and low SSE. In addition, the $q_{e2, cal}$ values predicted from the PSO model were also very parallel to the experimental values $q_{e, exp}$, for all the tested concentra-

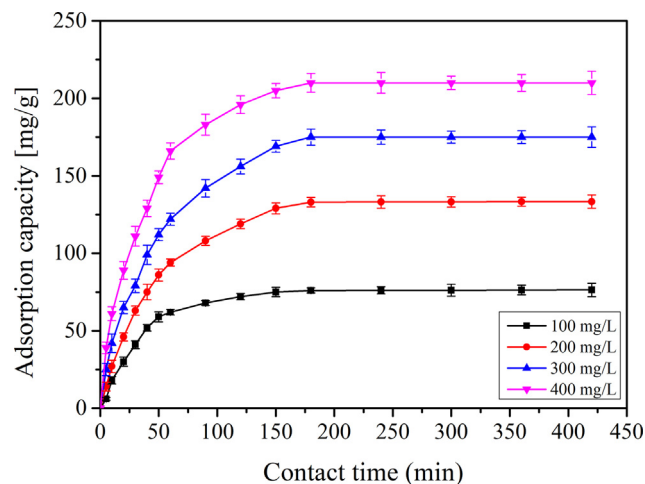


Fig. 8. Effect of contact time on the adsorption of CR onto Fe_3O_4 -PSP [initial dye concentration = 100–400 mg/L; dye volume = 30 mL; pH = 5.0; shaking speed = 200 rpm; temperature = 303 K].

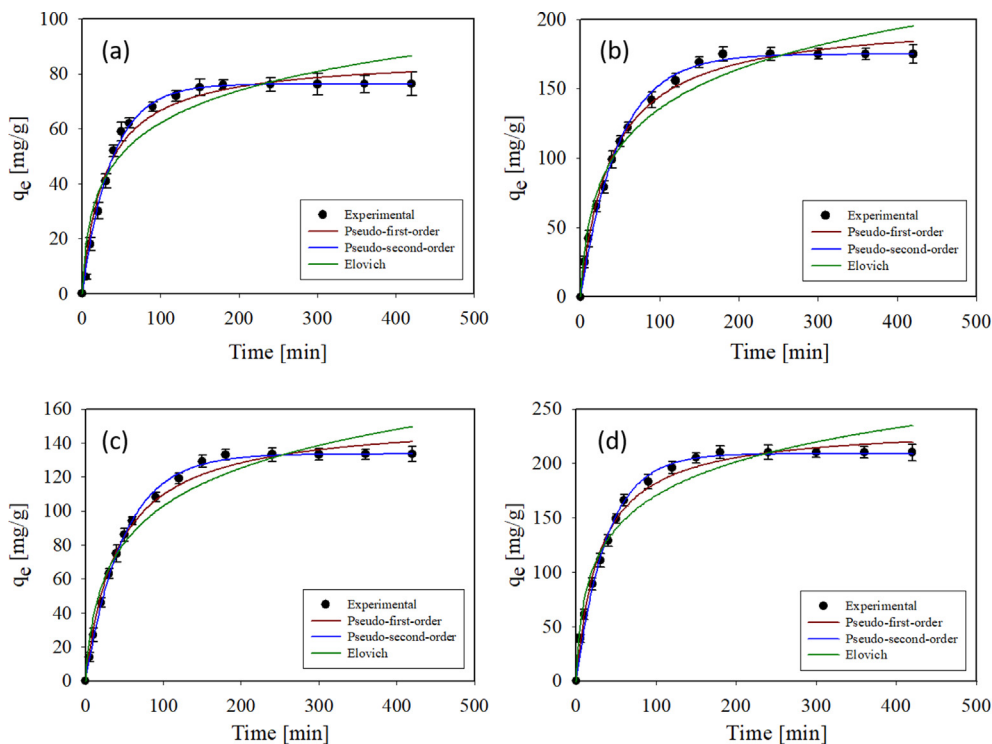


Fig. 9. Kinetic plots for the adsorption of CR onto Fe₃O₄-PSP at different initial concentrations: (a) 100 mg/L, (b) 200 mg/L, (c) 300 mg/L, and (d) 400 mg/L [adsorbent mass = 0.05 g; dye volume = 30 mL; pH = 5.0; shaking speed = 200 rpm; temperature = 303 K].

Table 2
Kinetic parameters for the adsorption of CR onto Fe₃O₄-PSP at various initial dye concentrations.

| Kinetic Model | Parameters | Concentration of CR solution (mg/L) | | | |
|---------------------|----------------------|-------------------------------------|--------|---------|---------|
| | | 100 | 200 | 300 | 400 |
| Experimental value | $q_{e, exp}$ (mg/g) | 76.41 | 133.35 | 175.05 | 210.63 |
| Pseudo-first-order | $q_{e1, cal}$ (mg/g) | 86.32 | 154.32 | 201.25 | 234.82 |
| | k_1 (1/min) | 0.0269 | 0.0208 | 0.0205 | 0.0261 |
| | R^2 | 0.9817 | 0.9866 | 0.9790 | 0.9735 |
| | SSE | 3.7512 | 4.4377 | 5.5675 | 6.6354 |
| | | | | | |
| Pseudo-second-order | $q_{e2, cal}$ (mg/g) | 76.25 | 133.44 | 174.91 | 208.75 |
| | k_2 (g/mg min) | 0.0042 | 0.0023 | 0.0015 | 0.00009 |
| | R^2 | 0.9972 | 0.9985 | 0.9951 | 0.9963 |
| | SSE | 1.5124 | 1.9033 | 3.3585 | 4.9069 |
| | | | | | |
| Elovich | α (mg/g min) | 6.1672 | 6.993 | 9.9915 | 19.1 |
| | β (g/mg) | 0.0579 | 0.0300 | 0.0236 | 0.0221 |
| | R^2 | 0.9307 | 0.9613 | 0.9664 | 0.9585 |
| | SSE | 7.3056 | 9.5144 | 11.3778 | 14.693 |

tions. This suggests that the CR adsorption onto Fe₃O₄-PSP is regulated by chemisorption. Furthermore, it can be seen that while the values of q_t rise with increasing C_0 , k_2 decreases with rising C_0 (Table 2). This may have something to do with the mass transfer driving force and C_0 . Because there are so many solute molecules at high C_0 , the mass transfer rate toward the biosorbent surface is faster, resulting in a higher driving force for the solute to breach the biosorbent boundary layer, allowing for more solute molecules to be adsorbed. When a significant number of solute molecules bind to the adsorbent's external surface empty sites, the diffusion rate of the remaining solute molecules in the bulk solution slows. The subsequent adsorption phase occurs when the solute molecules penetrate into the inner porous adsorbent matrix after all of the surface sites have been occupied [45]. The Elovich model is used to describe PSO and chemisorptive kinetics under the premise that the surface of solid systems is energetically heterogeneous. Table 2 shows the rising α values and falling β values as the CR concentration increases for Fe₃O₄-PSP. This lowering of β

values with the increase in initial CR concentration at the variable time depicted the chemisorptive behavior of CR onto the Fe₃O₄-PSP [46].

To further investigate the adsorption mechanisms, the intra-particle diffusion (IPD) kinetic model, based on Weber and Morris' theory, was fitted to the experimental data using the following equation:

$$q_t = K_{id}(t)^{0.5} + C \tag{13}$$

Fig. 10 illustrates the plot of the IPD kinetic model for the adsorption of CR on the Fe₃O₄-PSP for different initial dye concentrations. For all initial CR concentrations, the figure depicts three stages with varying slopes. External diffusion, which reflects the diffusion of CR molecules from the liquid phase to the biosorbent surface, is the first sharply linear phase. The second linear phase is IPD, which represents CR molecules entering the pores from the external surface. The last phase, which takes a long time to achieve, is considered to be the final adsorption/desorption equi-

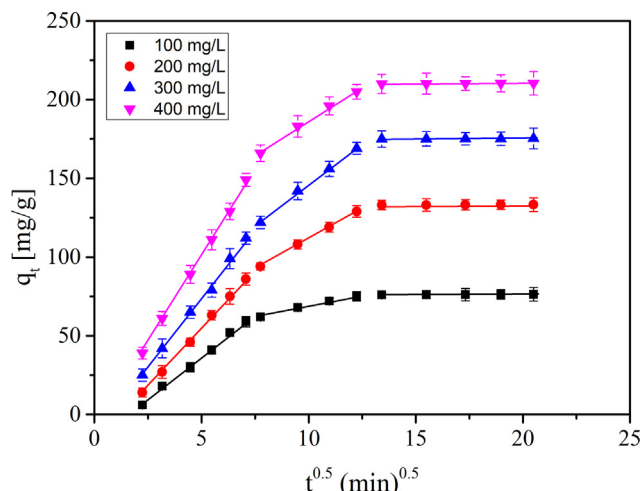


Fig. 10. Intra-particle diffusion model for CR adsorption onto Fe₃O₄-PSP [initial dye concentration = 100–400 mg/L; dye volume = 30 mL; pH = 5.0; shaking speed = 200 rpm; temperature = 303 K].

librium. When the regression curve of q_t against $t^{0.5}$ is linear and passes through the origin, IPD is the sole rate-limiting step [47]. However, the linear portion of plots at each individual concentration did not pass through the origin, implying that IPD was not only the rate-limiting step in CR adsorption onto the Fe₃O₄-PSP and that other kinetics may control the adsorption rate concurrently. The constants of IPD (k_{id} and C) for all steps are presented in Table 3. The reaction constant k_{id} decreased following the order k_{id1} (first stage) > k_{id2} (second stage) > k_{id3} (third stage) with raising the adsorption time during the diffusion process and simultaneously the values of C rose following the sequence of $C_1 < C_2 < C_3$, suggesting a rise in the boundary layer thickness. Therefore, as a consequence of the stronger interaction between CR and Fe₃O₄-PSP at upper stages, a thicker boundary layer may further decrease the reaction rate [48]. On the other hand, the k_{id} values rose with initial CR concentration, which may be due to the increasing impact of the driving force, which produces a decrease in CR diffusion in the boundary layer as well as an increase in diffusion in the solid [31].

3.7. Adsorption isotherms

Adsorption isotherm models were primarily utilized to explain the distribution of adsorbate molecules on the adsorbent surface at equilibrium between the liquid and solid phases. To correlate the experimental equilibrium adsorption data, the four two-parameter non-linear isotherms Langmuir, Freundlich, Temkin, and D-R models were employed.

The Langmuir adsorption, which is the monolayer, is assumed to quickly reduce the intermolecular interactions at a distance and thus predicts the monolayer coverage of adsorbate on the external surface of the sorbent [28]. The expression of the non-linear Langmuir isotherm model is shown as below:

$$q_e = \frac{q_{max}K_L C_e}{1 + K_L C_e} \tag{14}$$

The maximal monolayer adsorption capacity (q_{max}) of CR calculated using the Langmuir isotherm model was 216.9 mg/g. The main aspects of the Langmuir isotherm factors may be utilized to estimate the affinity between adsorbate and biosorbent using the separation factor or dimensionless equilibrium factor, R_L , which is described by the following expression:

$$R_L = \frac{1}{(1 + K_L C_o)} \tag{15}$$

R_L value shows the feasibility of the sorption process, where the adsorption is: when ($R_L > 1.0$), it is unfavorable; when ($R_L = 1.0$), it is linear; when ($0 < R_L < 1.0$), it is favorable; and when ($R_L = 0$), it is irreversible. The achieved R_L values at a different initial concentration of CR dye are presented in Table 4. According to Table 4, the obtained R_L values were between 0 and 1.0, demonstrating that the adsorption of CR onto Fe₃O₄-PSP is a favorable process.

The Freundlich isotherm is based on the equilibrium relationship between heterogeneous surfaces. This isotherm is derived from the premise that adsorption sites are spread exponentially in terms of adsorption heat. It also signifies that the stronger adsorption sites are saturated first and that adsorption strength declines as site occupancy rises [49]. The Freundlich equation in its non-linear version is written as:

$$q_e = K_f C_e^{1/n} \tag{16}$$

This model's n value is in the range of 1.0–10.0, suggesting favorable adsorption. According to Table 4, the value of n for this model is in the range of 1.0–10.0, and thus the derived results indicate that the adsorption of CR onto Fe₃O₄-PSP was found to be very favorable, implying a multilayer phenomenon.

The D-R isotherm model takes into account the adsorption mechanism as a consequence of the Gaussian energy distribution of adsorbates on a heterogeneous surface for adsorption [50]. The D-R equation may be stated in non-linear form as follows:

$$q_e = q_s \exp(-K \varepsilon^2) \varepsilon = RT \ln \left(1 + \frac{1}{C_e} \right) \tag{18}$$

The mean free adsorption energy, E , is calculated using Eq. (15):

$$E = \frac{1}{\sqrt{2K}} \tag{19}$$

The amount of E can determine the adsorption mechanism: adsorption is controlled by the ion-exchange mechanism at $E = 8.0$ – 16.0 kJ/mol; at $E < 8.0$ kJ/mol, physical bonds like as Van der Waals force and hydrogen bonding control adsorption; at $E > 16.0$ kJ/mol, the particle diffusion mechanism may influence the sorption process [51]. Based on the listed data in Table 4, the calculated value of E was determined to be < 8.0 kJ/mol; it suggests that the adsorption of CR onto Fe₃O₄-PSP may be affected by physical forces.

Temkin model applies to adsorption on heterogeneous solid adsorbents and liquid adsorbates because it explicitly considers adsorbent/adsorbate interaction by presuming the heat of all mole-

Table 3
Weber-Morris model parameters for the adsorption of CR onto Fe₃O₄-PSP.

| Initial CR dye Conc. (mg/L) | Weber and Morris model | | | | | |
|-----------------------------|--------------------------------------|--------------|--------------------------------------|--------------|--------------------------------------|--------------|
| | k_{id1} (mg/g min ^{0.5}) | C_1 (mg/g) | k_{id2} (mg/g min ^{0.5}) | C_2 (mg/g) | k_{id3} (mg/g min ^{0.5}) | C_3 (mg/g) |
| 100 | 10.881 | 17.7 | 2.889 | 40.04 | 0.0396 | 75.31 |
| 200 | 15.029 | 20.17 | 7.753 | 34.12 | 0.0433 | 132.43 |
| 300 | 17.834 | 15.13 | 10.378 | 42.34 | 0.0511 | 174.47 |
| 400 | 22.343 | 10.73 | 14.723 | 99.34 | 0.0529 | 209.35 |

Table 4
Langmuir, Freundlich, Temkin, and D-R isotherm models and separation factors for the adsorption of CR onto Fe₃O₄-PSP at 303 K.

| Adsorption isotherm | Parameter | Value |
|-----------------------------|---|---------|
| Langmuir | q_m (mg/g) | 216.9 |
| | K_L (L/mg) | 0.07397 |
| | R^2 | 0.9962 |
| | χ^2 | 27.16 |
| Freundlich | K_f (mg/g) | 78.94 |
| | n | 6.0953 |
| | R^2 | 0.9499 |
| | χ^2 | 216.46 |
| Temkin | B_T (J/mol) | 86.37 |
| | A_T (L/mg) | 3.7378 |
| | R^2 | 0.9304 |
| | χ^2 | 357.62 |
| Dubinin-Radushkevich | q_s (mg/g) | 207.4 |
| | K (mol ² /J ²) | 0.02333 |
| | E (kJ/mol) | 4.629 |
| | R^2 | 0.5966 |
| | χ^2 | 1255.1 |
| Separation factor (R_L) | C_o (mg/L) | R_L |
| | 100 | 0.12 |
| | 200 | 0.063 |
| | 300 | 0.043 |
| | 400 | 0.033 |
| | 500 | 0.026 |
| | 700 | 0.019 |
| 1000 | 0.013 | |

cules' adsorption in the layer decreases linearly rather than logarithmically with adsorbent surface coverage [52]. The non-linearized version of the Temkin model is as follows:

$$q_e = B_T \ln(A_T C_e) \tag{20}$$

$$q_e = B_T \ln(A_T) + B_T \ln(C_e) B_T = \frac{RT}{b_T} \tag{22}$$

The values of B_T and A_T constants of the Temkin isotherm parameter were estimated to be 86.37 (J/mol) and 3.738 (L/mg), respectively. Thus, the value of B_T was lower than 8.0 kJ/mol, indicating that the heat of adsorption of CR onto Fe₃O₄-PSP is a physisorption process [53].

By comparing the R^2 (correlation coefficient) values, it was found that the experimental data fitted better to the Langmuir model, with a value of 0.9962 than D-R, Freundlich, and Temkin isotherm model with values of 0.5966, 0.9499, and 0.9304, respectively. According to the concluded values of R^2 (higher) and χ^2 (lower), the favorability of the isotherm models may obey the order: Langmuir > Freundlich > Temkin > D-R. The Langmuir model's superiority may be attributed to the monolayer distribution of CR dye on the homogeneous active sites present on the Fe₃O₄-PSP surface. Therefore, the CR adsorption onto Fe₃O₄-PSP is monolayer adsorption onto a surface containing a finite number of identical adsorption sites. Two-parameter non-linearized versions of the Freundlich, Temkin, D-R and Langmuir isotherm models were applied, and results are shown in Fig. 11 and Table 4.

3.8. Comprehensive comparison or performance evaluation

Table 5 shows the adsorption capability of Fe₃O₄-PSP with various adsorbents described in previous studies [38,54–65] for eliminating CR. When compared to the other biosorbents mentioned, the adsorption capacity of the CR dye molecules on Fe₃O₄-PSP was extremely high. The existence of surface interactions like hydrogen bonding and electrostatic interactions contributed to the high dye removal capacity. Furthermore, using an external magnetic field, the Fe₃O₄-PSP may be regenerated and readily separated from an aqueous solution without any weight loss. As a

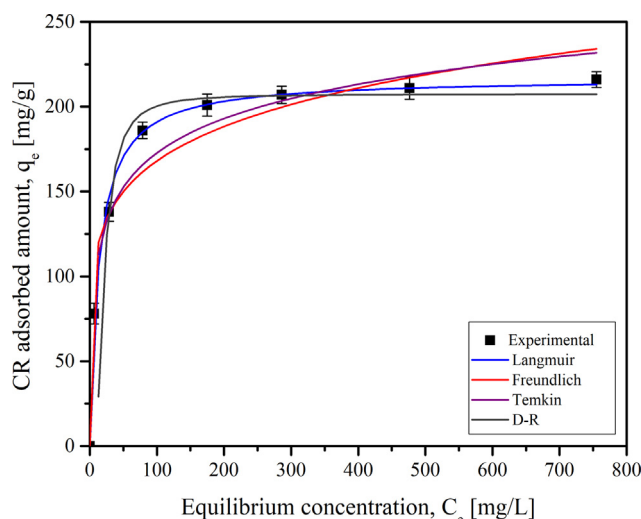


Fig. 11. Non-linear fitting of the Langmuir, Freundlich, Temkin, and D-R isotherm models for the adsorption of CR onto Fe₃O₄-PSP [initial dye concentration = 100–1000 mg/L; dye volume = 30 mL; pH = 5.0; shaking speed = 200 rpm; time = 180 min; temperature = 303 K].

Table 5
Comparison of the CR dye adsorption capacity of Fe₃O₄-PSP with various adsorbents.

| Adsorbent | q_{max} (mg/g) | pH | Reference |
|--|------------------|-----|---------------|
| MgFe ₂ O ₄ -NH ₂ NPs | 71.4 | 6.0 | [38] |
| CABI nano-goethite | 181.1 | 3.0 | [54] |
| m-cell/Fe ₃ O ₄ /ACCs | 66.09 | 4.0 | [55] |
| Zeolites modified with DAAO | 69.94 | 6.0 | [56] |
| CTAB-modified magnetite nanoparticles | 93.46 | - | [57] |
| Magnetic Fe ₃ O ₄ @graphene nanocomposite | 33.66 | - | [58] |
| Fe ₃ O ₄ -TSPED-Tryptophan | 183.15 | 3.0 | [59] |
| Fe ₃ O ₄ /Bi ₂ S ₃ MSs | 92.24 | - | [60] |
| Fe ₃ O ₄ -GG nanocomposite | 60.24 | - | [61] |
| Fe ₃ O ₄ @SiO ₂ @Zn-TDPAT | 17.73 | 5.0 | [62] |
| ZrO ₂ microspheres | 59.5 | 7.0 | [63] |
| Fe ₃ O ₄ /NiO nanocomposite | 210.78 | 5.0 | [64] |
| Iron-grafted clinoptilolite | 36.70 | 6.5 | [65] |
| Fe ₃ O ₄ loaded papaya seed powder | 216.9 | 5.0 | Present study |

result, it is fair to infer that Fe₃O₄-PSP is a promising adsorbent for extracting CR from an aqueous media.

3.9. Effect of temperature and Van't Hoff plot (thermodynamic studies)

Temperature influences the mobility and solubility of dye molecules in aqueous solutions, as well as the surface properties of the biosorbent, making it a critical element in the adsorption process. Fig. 12(a) depicts the effect of temperature on the adsorption of CR on Fe₃O₄-PSP. The tests were carried out at four temperatures (303, 313, 323, and 333 K) with a constant initial dye concentration of 100 mg/L and pH of 5.0. The experimental findings showed that CR adsorption onto Fe₃O₄-PSP was endothermic, as the adsorption capacity raised with increasing temperature. The viscosity of the solution reduces as temperature rises, increasing the rate of transfer of adsorbate molecules over the phase boundary and into the interior pores of the solid sorbent and so improving the sorbent's adsorptive capabilities. At higher temperatures, the phenomenon may also be ascribed to the adsorbent's pore size increase and potential surface activation [46]. According to the findings, the

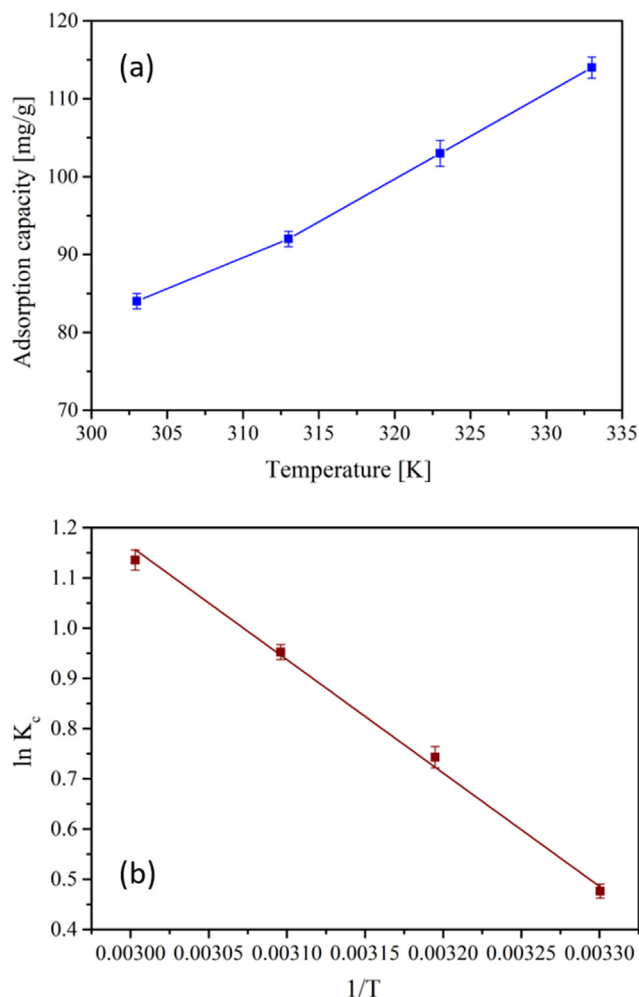


Fig. 12. (a) Effect of temperature on the adsorption of CR onto Fe₃O₄-PSP [initial dye concentration = 100 mg/L; dye volume = 30 mL; pH = 5.0; shaking speed = 200 rpm; time = 180 min; temperature = 303–333 K] and (b) Van't Hoff plot ($1/T$ versus $\ln K_c$) for the adsorption of CR onto Fe₃O₄-PSP [initial dye concentration = 100 mg/L; dye volume = 30 mL; pH = 5.0; time = 180 min; shaking speed = 200 rpm; temperature = 303–333 K].

sorption process of CR onto Fe₃O₄-PSP is highly temperature-dependent.

The temperature dependency of the adsorption process as well as the spontaneity of the adsorption of CR dye molecules on Fe₃O₄-PSP are investigated using adsorption thermodynamics. The thermodynamic parameter terms such as ΔH° , ΔS° , and ΔG° can be evaluated from the following Eqs. (23) - (26):

$$\Delta G^\circ = \Delta H^\circ - T\Delta S^\circ \quad (23)$$

$$\Delta G^\circ = -RT\ln K_c \quad (24)$$

$$K_c = \frac{C_{Ae}}{C_e} \ln K_c = -\frac{\Delta G^\circ}{RT} = -\frac{\Delta H^\circ}{RT} + \frac{\Delta S^\circ}{R} \quad (26)$$

The magnitude of ΔH° and ΔS° was derived from the slope and intercept of $1/T$ vs $\ln K_c$ (Van't Hoff plot), as illustrated in Fig. 12(b). The derived values of the ΔH° , ΔS° , and ΔG° are summarized in Table 6. The positive ΔH° value indicates that the endothermic nature of the reaction involved during the adsorption process. In addition, the magnitude of ΔH° may give an idea about the type of adsorption. The heat evolved during physisorption, for example, is of the same order of magnitude as condensation heats, i.e.,

2.10–20.90 kJ/mol. Chemisorption heats, on the other hand, typically range between 80.0 and 200.0 kJ/mol [66]. The heat of reaction of the adsorption process of CR onto Fe₃O₄-PSP was 18.4 kJ/mol; this implied that the adsorption process was by physisorption. The positive value of ΔS° (64.8 J/mol K) denotes the prepared Fe₃O₄-PSP adsorbent's good affinity for the CR and increased random degree at the interface layer between solid and liquid during adsorption, implying that adsorption is more favorable at higher temperatures [67]. The negative ΔG° values (−1.1997 to −3.1439 kJ/mol) obtained at all temperatures (303–333 K) indicate that the adsorption process was spontaneous and feasible. Furthermore, the ΔG° value decreased as the reaction temperature raised, suggesting that the adsorption mechanism of CR onto Fe₃O₄-PSP is more favorable at upper temperatures [68]. Thermodynamic parameters for the adsorption of CR on Fe₃O₄-PSP is compared with previously reported other adsorbents (Table 6) [18,54,62,64,69].

3.10. Desorption and reusability studies

In order to achieve sustainable applications, adsorbents need to be regenerated and recycled after the adsorption process. In this experiment, 100 mg/L of CR is treated with 0.05 g adsorbent. After completing the adsorption process, batch desorption tests were conducted using 0.1 M solution of different diluents NaCl, NaOH, CH₃COOH, HCl, and H₂O, in the same conditions. Fig. 13(a) shows the comparison between the other desorption efficiencies. NaOH showed the highest desorption efficiency of 96.3%, while the use of NaCl, CH₃COOH, HCl, and H₂O resulted in low desorption efficiency, 72.6, 54.2, 38.3, and 24.8%, respectively. Accordingly, 0.1 M NaOH was used as the most suitable desorbing agent. It is worth noting that increasing the NaOH concentration (0.1–1.0 M) leads to a reduction in desorption efficiency (96.3–29.7%), which is caused by the degradation of active sites on the surface of Fe₃O₄-PSP (Fig. 13(b)). The CR adsorption/desorption was analyzed for five cycles with 0.1 M NaOH, and the findings are shown in Fig. 13(c). The CR adsorption efficiency dropped from 93.1 to 91.2% between the first and second cycles. In the fifth cycle, the CR adsorption efficiency dropped to 84.8% (Fig. 13(c)). This may be attributed to the Fe₃O₄-PSP's decreasing CR efficiency, which showed a decrease in regeneration efficiency for continuous cycles. The decrease, on the other hand, may be attributable to a reduction in the number of binding sites on the Fe₃O₄-PSP surface [70]. Additionally, the saturation of the available binding sites on the adsorbent by CR molecules could have occurred. In terms of the desorption process, CR desorption efficiency had similarly dropped from 96.3% in the first cycle to 87.7% in the fifth cycle (Fig. 13(c)). These findings showed that Fe₃O₄-PSP has higher reusability and is an excellent adsorbent for wastewater treatment. As a result, the adsorbent's economic viability is suitable for large-scale industrial applications.

3.11. Proposed adsorption mechanism

Adsorption performance is influenced by a variety of parameters, including solution pH, surface morphology, roughness, surface area, dye structures, adsorbent-adsorbate interactions, adsorbent surface charge, and active sites, among others [71,72]. Fe₃O₄-PSP contains huge amounts of -COOH, -NH₂, and -OH functional groups, making it an ideal biosorbent for eliminating anionic CR contaminants from the liquid phase. In an acidic medium, these groups are readily protonated, allowing them to strongly adsorb anionic CR dye via strong electrostatic interactions and hydrogen bonding, as illustrated in Fig. 14.

Table 6
Comparison of thermodynamic parameters of various adsorbents for CR.

| Adsorbent | Temp. [K] | Thermodynamic parameters | | | Reference |
|---|-----------|---------------------------|----------------------------|---------------------------|---------------|
| | | ΔG° (kJ/mol) | ΔS° (J/mol K) | ΔH° (kJ/mol) | |
| Alkali-soluble polysaccharide | 303 | -5.135 | 95 | 23.584 | [18] |
| | 318 | -6.556 | | | |
| | 333 | -7.977 | | | |
| | 343 | -8.924 | | | |
| CABl nano-goethite | 293 | -0.099 | 83 | 24.4 | [54] |
| | 303 | -0.902 | | | |
| | 313 | -1.673 | | | |
| | 323 | -2.508 | | | |
| Fe ₃ O ₄ @SiO ₂ @Zn- TDPAT | 298 | -4.049 | 94.61 | 24.145 | [62] |
| | 308 | -4.995 | | | |
| | 318 | -5.942 | | | |
| Fe ₃ O ₄ /NiO nanocomposite | 293.15 | -2.9649 | 104.71 | 27.69 | [64] |
| | 303.15 | -4.0399 | | | |
| | 313.15 | -5.2601 | | | |
| | 323.15 | -6.0361 | | | |
| PPy-Fe ₃ O ₄ -SW | 303 | -7.2301 | 186.3 | 48.394 | [69] |
| | 308 | -7.7879 | | | |
| | 313 | -8.934 | | | |
| | 318 | -9.6151 | | | |
| | 323 | -11.801 | | | |
| | 328 | -11.986 | | | |
| | 333 | -12.172 | | | |
| Fe ₃ O ₄ loaded papaya seed powder | 303 | -1.1997 | 64.8 | 18.4 | Present study |
| | 313 | -1.9332 | | | |
| | 323 | -2.5577 | | | |
| | 333 | -3.1439 | | | |

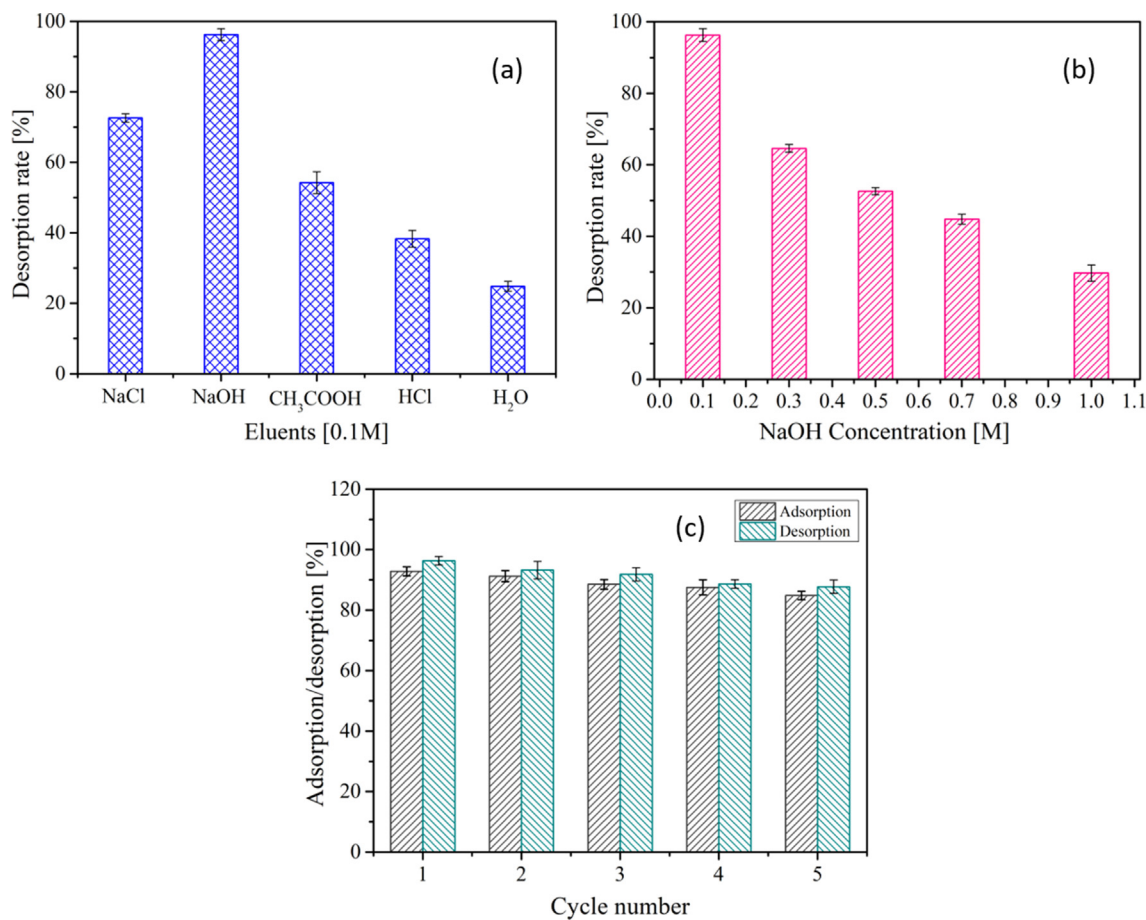


Fig. 13. (a) Desorption of CR dye from loaded Fe₃O₄-PSP using various eluents (0.1 M) [adsorbent mass = 0.05 g; contact time = 180 min; temperature = 303 K; volume of eluent = 30 mL; shaking speed = 200 rpm], (b) Effect of NaOH concentration on desorption efficiency [adsorbent mass = 0.05 g; contact time = 180 min; temperature = 303 K; volume = 30 mL, NaOH concentration = 0.1–1.0 M; shaking speed = 200 rpm], and (c) Regeneration performance of Fe₃O₄-PSP onto CR in five successive cycles of adsorption-desorption [adsorbent mass = 0.05 g; contact time = 180 min; temperature = 303 K; volume of eluent = 30 mL; shaking speed = 200 rpm].

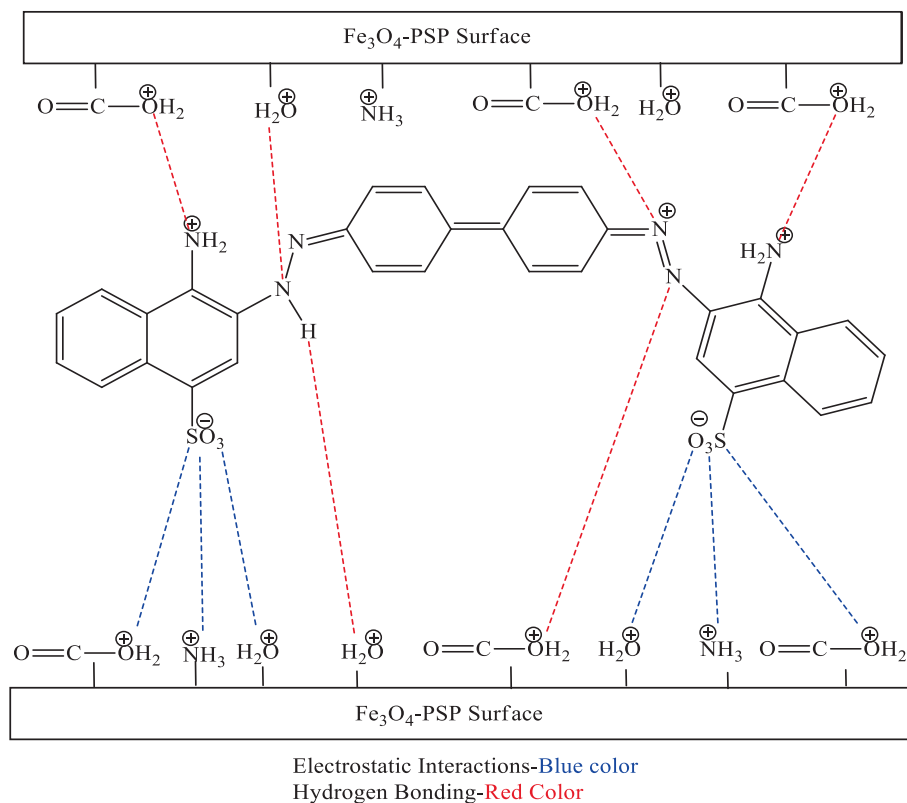


Fig. 14. Mechanism of CR adsorption onto Fe₃O₄-PSP surface at pH 5.0.

- o The electrostatic interactions between the positively charged groups ($-\text{OH}_2^+$, $-\text{NH}_3^+$, and $-\text{COOH}_2^+$) available on the Fe₃O₄-PSP surface and negatively charged $-\text{SO}_3^-$ groups of the CR dye.
- o The hydrogen bonding between H atom available on the surface of Fe₃O₄-PSP and N atoms in the CR dye structure.

Therefore, it can be concluded that electrostatic interactions and hydrogen bonding play a vital role in the adsorption of CR onto Fe₃O₄-PSP.

4. Conclusions

Magnetic Fe₃O₄-PSP has been successfully synthesized and utilized as a potential sorbent for the removal of CR. The effect of adsorption variables, such as CR dye concentration, Fe₃O₄-PSP mass, contact time, temperature, and pH edge, was considered and optimized. The prepared Fe₃O₄-PSP was comprehensively characterized. The results of FT-IR, EDX, and XRD indicated that Fe₃O₄ nanoparticles were well incorporated into the PSP surface. VSM results illustrated the biosorbent was easy to be recycled. The equilibrium data were best suited by the Langmuir isotherm model ($R^2 = 0.9962$), indicating a monolayer coverage. The maximum adsorption efficiency of the Fe₃O₄-PSP was observed to be 216.9 mg/g at pH 5.0 and 180 min. The R_L values also revealed that the adsorption is feasible. The kinetic modeling exhibited that the experimental findings fitted well with the PSO model ($R^2 > 0.9951$). A three-stage multi-linear plot was utilized to evaluate the diffusion process, demonstrating that IPD into mesopores may be a regulating step for CR adsorption but is not the only rate-limiting step. The main adsorption mechanism was chemisorption and may be accompanied by physisorption. The adsorption capacity rose when the temperature was raised, indicating that the adsorption process is endothermic. Hydrogen bonding and electrostatic interactions

play a dominant role in the adsorption of CR by Fe₃O₄-PSP. The thermodynamic behavioral aspects at various temperatures explained that CR adsorption by Fe₃O₄-PSP was spontaneous, feasible, and endothermic. After adsorption, an external magnetic field was used to separate the adsorbent from the aqueous media, and five adsorption/desorption cycle tests revealed that the Fe₃O₄-PSP for CR was extremely reusable. Because of all these findings, it may be concluded that the prepared Fe₃O₄-PSP can be employed as a low-cost, easily available precursor, satisfactory reusability, easy separation, and highly efficient adsorbent to remove dye-contaminated wastewater effluents.

CRediT authorship contribution statement

Venkata Subbaiah Munagapati: Writing – original draft, Data curation, Methodology, Conceptualization, Visualization, Formal analysis. **Hsin-Yu Wen:** Conceptualization, Validation, Visualization. **Anjani R.K. Gollakota:** Data curation, Formal analysis, Conceptualization. **Jet-Chau Wen:** Conceptualization, Supervision, Resources, Funding acquisition, Data curation, Writing – review & editing. **Chi-Min Shu:** Conceptualization, Validation, Writing – review & editing. **Kun-Yi Andrew Lin:** Data curation, Visualization, Writing – review & editing. **Zhong Tian:** Conceptualization. **Jhy-Horng Wen:** Conceptualization, Validation. **Guda Mallikarjuna Reddy:** Conceptualization, Visualization. **Grigory V. Zyryanov:** Conceptualization.

Declaration of Competing Interest

The authors declare that they have no known competing financial interests or personal relationships that could have appeared to influence the work reported in this paper.

Acknowledgement

The authors would like to acknowledge the research support from, MOST 107-2625-M-224-002, MOST 108-2625-M-224-005, and MOST 110-2625-M-224-001, by the Ministry of Science and Technology (MOST), Taiwan.

References

- M.T. Yagub, T.K. Sen, S. Afroz, H.M. Ang, Dye and its removal from aqueous solution by adsorption: a review, *Adv. Colloid Interface Sci.* 209 (2014) 172–184, <https://doi.org/10.1016/j.cis.2014.04.002>.
- A.K. Prajapati, M.K. Mondal, Development of CTAB modified ternary phase α - Fe_2O_3 - Mn_2O_3 - Mn_3O_4 nanocomposite as innovative super-adsorbent for Congo red dye adsorption, *J. Environ. Chem. Eng.* 9 (1) (2021) 104827, <https://doi.org/10.1016/j.jece.2020.104827>.
- M.L.G. Vieira, V.M. Esquerdo, L.R. Nobre, G.L. Dotto, L.A.A. Pinto, Glass beads coated with chitosan for the food azo dyes adsorption in a fixed bed column, *J. Ind. Eng. Chem.* 20 (5) (2014) 3387–3393, <https://doi.org/10.1016/j.jiec.2013.12.024>.
- R. Satheesh, K. Vignesh, M. Rajarajan, A. Suganthi, S. Sreekantan, M. Kang, B.S. Kwak, Removal of congo red from water using quercetin modified α - Fe_2O_3 nanoparticles as effective nano-adsorbent, *Mater. Chem. Phys.* 180 (2016) 53–65, <https://doi.org/10.1016/j.matchemphys.2016.05.029>.
- S. Khan, A. Malik, Toxicity evaluation of textile effluents and role of native soil bacterium in biodegradation of a textile dye, *Environ. Sci. Pollut. Res.* 25 (5) (2018) 4446–4458, <https://doi.org/10.1007/s11356-017-0783-7>.
- T.K. Roy, N.K. Mondal, Potentiality of Eichhornia shoots ash towards removal of Congo red from aqueous solution: isotherms, kinetics, thermodynamics and optimization studies, *Groundw. Sustain. Dev.* 9 (2019) 100269, <https://doi.org/10.1016/j.gsd.2019.100269>.
- C. Li, L. Zhang, H. Xia, J. Peng, S. Zhang, S. Cheng, J. Shu, Kinetics and isotherms studies for congo red adsorption on mesoporous Eupatorium adenophorum-based activated carbon via microwave-induced H_3PO_4 activation, *J. Mol. Liq.* 224 (2016) 737–744, <https://doi.org/10.1016/j.molliq.2016.10.048>.
- M. Makrygianni, Z.G. Lada, A. Manousou, C.A. Aggelopoulos, V. Deimede, Removal of anionic dyes from aqueous solution by novel pyrrolidinium-based Polymeric Ionic Liquid (PIL) as adsorbent: investigation of the adsorption kinetics, equilibrium isotherms and the adsorption mechanisms involved, *J. Environ. Chem. Eng.* 7 (3) (2019) 103163, <https://doi.org/10.1016/j.jece.2019.103163>.
- P.B. Santos, J.J. Santos, C.C. Corrêa, P. Corio, G.F.S. Andrade, Plasmonic photodegradation of textile dye Reactive Black 5 under visible light: a vibrational and electronic study, *J. Photochem. Photobiol. A Chem.* 371 (2019) 159–165, <https://doi.org/10.1016/j.jphotochem.2018.11.005>.
- A.S. Abdulhameed, A.K.T. Mohammad, A.H. Jawad, Application of response surface methodology for enhanced synthesis of chitosan tripolyphosphate/ TiO_2 nanocomposite and adsorption of reactive orange 16 dye, *J. Clean. Prod.* 232 (2019) 43–56, <https://doi.org/10.1016/j.jclepro.2019.05.291>.
- G. Akkaya, F. Güzel, Application of some domestic wastes as new low-cost biosorbents for removal of methylene blue: kinetic and equilibrium studies, *Chem. Eng. Commun.* 201 (4) (2014) 557–578, <https://doi.org/10.1080/00986445.2013.780166>.
- M. Kamranifar, M. Khodadadi, V. Samiei, B. Dehdashti, M. Noori Sepehr, L. Rafati, N. Nasseh, Comparison the removal of reactive red 195 dye using powder and ash of barberry stem as a low cost adsorbent from aqueous solutions: Isotherm and kinetic study, *J. Mol. Liq.* 255 (2018) 572–577, <https://doi.org/10.1016/j.molliq.2018.01.188>.
- J.N. Wekoye, W.C. Wanyonyi, P.T. Wangila, M.K. Tonui, Kinetic and equilibrium studies of Congo red dye adsorption on cabbage waste powder, *Environ. Chem. Ecotoxicol.* 2 (2020) 24–31, <https://doi.org/10.1016/j.enceco.2020.01.004>.
- B.T. Gemic, H.U. Ozel, H.B. Ozel, Removal of methylene blue onto forest wastes: adsorption isotherms, kinetics and thermodynamic analysis, *Environ. Technol. Innov.* 22 (2021) 101501, <https://doi.org/10.1016/j.eti.2021.101501>.
- C. Bhattacharjee, S. Dutta, V.K. Saxena, A review on biosorbent removal of dyes and heavy metals from wastewater using watermelon rind as biosorbent, *Environ. Adv.* 2 (2020) 100007, <https://doi.org/10.1016/j.ensadv.2020.100007>.
- A. Çelekli, A.I. Al-Nuaimi, H. Bozkurt, Adsorption kinetic and isotherms of Reactive Red 120 on Moringa oleifera seed as an eco-friendly process, *J. Mol. Struct.* 1195 (2019) 168–178, <https://doi.org/10.1016/j.molstruc.2019.05.106>.
- M. Tukaram Bai, O. Shaik, J. Kavitha, M.S. Hemanth Varma, N. Chittibabu, Biosorption of eosin yellow dye from aqueous solution using sugarcane bagasse: equilibrium, kinetics and thermodynamics, *Mater. Today Proc.* 26 (2019) 842–849, <https://doi.org/10.1016/j.matpr.2020.01.051>.
- J.K. Fatombi, S.A. Osseni, E.A. Idohou, I. Agani, D. Neumeyer, M. Verelst, R. Mauricot, T. Aminou, Characterization and application of alkali-soluble polysaccharide of Carica papaya seeds for removal of indigo carmine and Congo red dyes from single and binary solutions, *J. Environ. Chem. Eng.* 7 (5) (2019) 103343, <https://doi.org/10.1016/j.jece.2019.103343>.
- D.P. Rosa, R.R. Evangelista, A.L. Borges Machado, M.A.R. Sanches, J. Telis-Romero, Water sorption properties of papaya seeds (*Carica papaya* L.) formosa variety: an assessment under storage and drying conditions, *Lwt.* 138 (2021) 110458, <https://doi.org/10.1016/j.lwt.2020.110458>.
- U. Adie Gilbert, I. Unuabonah Emmanuel, A. Adeyemo Adebajo, G. Adeyemi Olalere, Biosorbent removal of Pb^{2+} and Cd^{2+} onto novel biosorbent: Defatted Carica papaya seeds, *Biomass Bioenergy.* 35 (2011) 2517–2525, <https://doi.org/10.1016/j.biombioe.2011.02.024>.
- G. Aravind, D. Bhowmik, S. Duraivel, G. Harish, Traditional and medicinal uses of carica papaya, *J. Med. Plants Stud.* 1 (2013) 7–15.
- M. Touihri, F. Guesmi, C. Hannachi, B. Hamrouni, L. Sellaloui, M. Badawi, J. Poch, N. Fiol, Single and simultaneous adsorption of $\text{Cr}(\text{VI})$ and $\text{Cu}(\text{II})$ on a novel Fe_3O_4 /pine cones gel beads nanocomposite: Experiments, characterization and isotherms modeling, *Chem. Eng. J.* 416 (2021) 129101, <https://doi.org/10.1016/j.cej.2021.129101>.
- K.G. Akpomie, J. Conradie, Biosorption and regeneration potentials of magnetite nanoparticle loaded Solanum tuberosum peel for celestine blue dye, *Int. J. Phytoremediation.* 23 (4) (2021) 347–361, <https://doi.org/10.1080/15226514.2020.1814198>.
- J.-L. Liu, W.-C. Qian, J.-Z. Guo, Y. Shen, B. Li, Selective removal of anionic and cationic dyes by magnetic Fe_3O_4 -loaded amine-modified hydrochar, *Bioresour. Technol.* 320 (2021) 124374, <https://doi.org/10.1016/j.biortech.2020.124374>.
- X. Liu, J. Tian, Y. Li, N. Sun, S. Mi, Y. Xie, Z. Chen, Enhanced dyes adsorption from wastewater via Fe_3O_4 nanoparticles functionalized activated carbon, *J. Hazard. Mater.* 373 (2019) 397–407, <https://doi.org/10.1016/j.jhazmat.2019.03.103>.
- D. Gautam, L. Saya, S. Hooda, Fe_3O_4 loaded chitin – a promising nano adsorbent for Reactive Blue 13 dye, *Environ. Adv.* 2 (2020) 100014, <https://doi.org/10.1016/j.ensadv.2020.100014>.
- A. Ebrahimi Pirbazari, E. Saberikhan, N. Gholami Ahmad Gorabi, Fe_3O_4 nanoparticles loaded onto wheat straw: an efficient adsorbent for Basic Blue 9 adsorption from aqueous solution, *Desalin. Water Treat.* 57 (2016) 4110–4121, doi:10.1080/19443994.2014.989918.
- J. Xie, R. Lin, Z. Liang, Z. Zhao, C. Yang, F. Cui, Effect of cations on the enhanced adsorption of cationic dye in Fe_3O_4 -loaded biochar and mechanism, *J. Environ. Chem. Eng.* 9 (4) (2021) 105744, <https://doi.org/10.1016/j.jece.2021.105744>.
- C. Prasad, S. Karlapudi, P. Venkateswarlu, I. Bahadur, S. Kumar, Green arbitrated synthesis of Fe_3O_4 magnetic nanoparticles with nanorod structure from pomegranate leaves and Congo red dye degradation studies for water treatment, *J. Mol. Liq.* 240 (2017) 322–328, <https://doi.org/10.1016/j.molliq.2017.05.100>.
- S. Yadav, A. Asthana, A.K. Singh, R. Chakraborty, S.S. Vidya, M.A.B.H. Susan, S.A. C. Carabineiro, Adsorption of cationic dyes, drugs and metal from aqueous solutions using a polymer composite of magnetic β -cyclodextrin/activated charcoal/Na alginate: isotherm, kinetics and regeneration studies, *J. Hazard. Mater.* 409 (2021) 124840, <https://doi.org/10.1016/j.jhazmat.2020.124840>.
- S. Maryam Hafezian, P. Biparva, A. Bekhradnia, S. Naser Azizi, Amine and thiol functionalization of SBA-15 nanoparticles for highly efficient adsorption of sulfuraphane, *Adv. Powder Technol.* 32 (3) (2021) 779–790, <https://doi.org/10.1016/j.apt.2021.01.025>.
- A.S. Eltaweil, H. Ali Mohamed, E.M. Abd El-Monaem, G.M. El-Subruiti, Mesoporous magnetic biochar composite for enhanced adsorption of malachite green dye: characterization, adsorption kinetics, thermodynamics and isotherms, *Adv. Powder Technol.* 31 (3) (2020) 1253–1263, <https://doi.org/10.1016/j.apt.2020.01.005>.
- F. Naseeruteen, N.S.A. Hamid, F.B.M. Suah, W.S.W. Ngah, F.S. Mehamod, Adsorption of malachite green from aqueous solution by using novel chitosan ionic liquid beads, *Int. J. Biol. Macromol.* 107 (2018) 1270–1277, <https://doi.org/10.1016/j.ijbiomac.2017.09.111>.
- A. Sarwar, M. Ali, A.H. Khoja, A. Nawar, A. Waqas, R. Liaquat, S.R. Naqvi, M. Asjid, Synthesis and characterization of biomass-derived surface-modified activated carbon for enhanced CO_2 adsorption, *J. CO_2 Util.* 46 (2021) 101476, <https://doi.org/10.1016/j.jcou.2021.101476>.
- S. Sahu, S. Pahi, S. Tripathy, S.K. Singh, A. Behera, U.K. Sahu, R.K. Patel, Adsorption of methylene blue on chemically modified lychee seed biochar: dynamic, equilibrium, and thermodynamic study, *J. Mol. Liq.* 315 (2020) 113743, <https://doi.org/10.1016/j.molliq.2020.113743>.
- S. Zhao, Y. Zhan, X. Wan, S. He, X. Yang, J. Hu, G. Zhang, Selective and efficient adsorption of anionic dyes by core/shell magnetic MWCNTs nano-hybrid constructed through facial polydopamine tailored graft polymerization: Insight of adsorption mechanism, kinetic, isotherm and thermodynamic study, *J. Mol. Liq.* 319 (2020) 114289, <https://doi.org/10.1016/j.molliq.2020.114289>.
- J. Zhou, W. Cai, Z. Yang, Q. Xia, J. Chen, J. Fan, C. Du, N. N-dimethylformamide assisted facile hydrothermal synthesis of boehmite microspheres for highly effective removal of Congo red from water, *J. Colloid Interface Sci.* 583 (2021) 128–138, <https://doi.org/10.1016/j.cis.2020.09.004>.
- C. Aopngan, J. Nonkumwong, S. Phumying, W. Promjantuek, S. Maensiri, P. Noisa, S. Pinitsoontorn, S. Ananta, L. Srisombat, Amine-functionalized and hydroxyl-functionalized magnesium ferrite nanoparticles for congo red adsorption, *ACS Appl. Nano Mater.* 2 (8) (2019) 5329–5341, <https://doi.org/10.1021/acsanm.9b01305>.
- R. Rahimi, H. Kerdari, M. Rabbani, M. Shafiee, Synthesis, characterization and adsorbing properties of hollow Zn- Fe_2O_4 nanospheres on removal of Congo red from aqueous solution, *Desalination* 280 (1–3) (2011) 412–418, <https://doi.org/10.1016/j.desal.2011.04.073>.
- Y. Shang, Y. Cui, R. Shi, P. Yang, J. Wang, Y. Wang, Regenerated $\text{WO}_{2.72}$ nanowires with superb fast and selective adsorption for cationic dye: Kinetics, isotherm, thermodynamics, mechanism, *J. Hazard. Mater.* 379 (2019) 120834, <https://doi.org/10.1016/j.jhazmat.2019.120834>.

- [41] P. Ilgin, H. Ozay, O. Ozay, Selective adsorption of cationic dyes from colored noxious effluent using a novel N-tert-butylmaleamic acid based hydrogels, *React. Funct. Polym.* 142 (2019) 189–198, <https://doi.org/10.1016/j.reactfunctpolym.2019.06.018>.
- [42] G. Sharma, M. Naushad, A. Kumar, S. Rana, S. Sharma, A. Bhatnagar, F.J. Stadler, A.A. Ghfar, M.R. Khan, Efficient removal of coomassie brilliant blue R-250 dye using starch/poly(alginate acid-cl-acrylamide) nanohydrogel, *Process Saf. Environ. Prot.* 109 (2017) 301–310, <https://doi.org/10.1016/j.psep.2017.04.011>.
- [43] L.e. Bo, F. Gao, Shuangbao, Ya.a. Bian, Z. Liu, Y. Dai, A novel adsorbent *Auricularia Auricular* for the removal of methylene blue from aqueous solution: Isotherm and kinetics studies, *Environ. Technol. Innov.* 23 (2021) 101576, <https://doi.org/10.1016/j.eti.2021.101576>.
- [44] A.R.K. Gollakota, V.S. Munagapati, S. Gautam, J.C. Wen, C.M. Shu, Hydrothermal tuning of morphology of aluminophosphate (AlPO₄-14) framework for the adsorption of Rhodamine 6G dye, *Adv. Powder Technol.* 32 (2021) 3002–3015, <https://doi.org/10.1016/j.apt.2021.06.015>.
- [45] A. Andreas, Z.G. Winata, S.P. Santoso, A.E. Angkawijaya, M. Yuliana, F.E. Soetaredjo, S. Ismadji, H.-Y. Hsu, A.W. Go, Y.-H. Ju, Biocomposite hydrogel beads from glutaraldehyde-crosslinked phytochemicals in alginate for effective removal of methylene blue, *J. Mol. Liq.* 329 (2021) 115579, <https://doi.org/10.1016/j.molliq.2021.115579>.
- [46] A. Thirunavukkarasu, K. Muthukumar, R. Nithya, Adsorption of acid yellow 36 onto green nanoceria and amine functionalized green nanoceria: comparative studies on kinetics, isotherm, thermodynamics, and diffusion analysis, *J. Taiwan Inst. Chem. Eng.* 93 (2018) 211–225, <https://doi.org/10.1016/j.jtice.2018.07.006>.
- [47] G. Yang, H. Chen, H. Qin, Y. Feng, Amination of activated carbon for enhancing phenol adsorption: Effect of nitrogen-containing functional groups, *Appl. Surf. Sci.* 293 (2014) 299–305, <https://doi.org/10.1016/j.apsusc.2013.12.155>.
- [48] B. Tanhaei, A. Ayati, E. Iakovleva, M. Sillanpää, Efficient carbon interlayered magnetic chitosan adsorbent for anionic dye removal: synthesis, characterization and adsorption study, *Int. J. Biol. Macromol.* 164 (2020) 3621–3631, <https://doi.org/10.1016/j.ijbiomac.2020.08.207>.
- [49] F.E. Titchou, R.A. Akbour, A. Assabane, M. Hamdani, Removal of cationic dye from aqueous solution using Moroccan pozzolana as adsorbent: isotherms, kinetic studies, and application on real textile wastewater treatment, *Groundw. Sustain. Dev.* 11 (2020) 100405, <https://doi.org/10.1016/j.gsd.2020.100405>.
- [50] H.A. Kiwaan, F.S. Mohamed, N.A. El-Ghamaz, N.M. Beshry, A.A. El-Bindary, Experimental and electrical studies of Na-X zeolite for the adsorption of different dyes, *J. Mol. Liq.* 332 (2021) 115877, <https://doi.org/10.1016/j.molliq.2021.115877>.
- [51] H. Alrobei, M.K. Prashanth, C.R. Manjunatha, C.B.P. Kumar, C.P. Chitranu, P.D. Shivaramu, K.Y. Kumar, M.S. Raghu, Adsorption of anionic dye on eco-friendly synthesised reduced graphene oxide anchored with lanthanum aluminate: Isotherms, kinetics and statistical error analysis, *Ceram. Int.* 47 (7) (2021) 10322–10331, <https://doi.org/10.1016/j.ceramint.2020.07.251>.
- [52] S.K. Low, M.C. Tan, Dye adsorption characteristic of ultrasound pre-treated pomelo peel, *J. Environ. Chem. Eng.* 6 (2) (2018) 3502–3509.
- [53] E. Wibowo, M. Rokhmat, Sutisna, Khairurrijal, M. Abdullah, Reduction of seawater salinity by natural zeolite (Clinoptilolite): Adsorption isotherms, thermodynamics and kinetics, *Desalination* 409 (2017) 146–156, <https://doi.org/10.1016/j.desal.2017.01.026>.
- [54] V.S. Munagapati, D.S. Kim, Equilibrium isotherms, kinetics, and thermodynamics studies for congo red adsorption using calcium alginate beads impregnated with nano-goethite, *Ecotoxicol. Environ. Saf.* 141 (2017) 226–234, <https://doi.org/10.1016/j.ecoenv.2017.03.036>.
- [55] H.-Y. Zhu, Y.-Q. Fu, R. Jiang, J.-H. Jiang, L. Xiao, G.-M. Zeng, S.-L. Zhao, Y. Wang, Adsorption removal of congo red onto magnetic cellulose/Fe₃O₄/activated carbon composite: Equilibrium, kinetic and thermodynamic studies, *Chem. Eng. J.* 173 (2) (2011) 494–502, <https://doi.org/10.1016/j.cej.2011.08.020>.
- [56] S. Liu, Y. Ding, P. Li, K. Diao, X. Tan, F. Lei, Y. Zhan, Q. Li, B. Huang, Z. Huang, Adsorption of the anionic dye Congo red from aqueous solution onto natural zeolites modified with N, N-dimethyl dehydroabietylamine oxide, *Chem. Eng. J.* 248 (2014) 135–144, <https://doi.org/10.1016/j.cej.2014.03.026>.
- [57] E. Saksornchai, J. Kavinchan, S. Thongtem, T. Thongtem, Simple wet-chemical synthesis of superparamagnetic CTAB-modified magnetite nanoparticles using as adsorbents for anionic dye Congo red removal, *Mater. Lett.* 213 (2018) 138–142, <https://doi.org/10.1016/j.matlet.2017.11.015>.
- [58] Y. Yao, S. Miao, S. Liu, L.P. Ma, H. Sun, S. Wang, Synthesis, characterization, and adsorption properties of magnetic Fe₃O₄@graphene nanocomposite, *Chem. Eng. J.* 184 (2012) 326–332, <https://doi.org/10.1016/j.cej.2011.12.017>.
- [59] J.K. Sahoo, S.K. Paikra, M. Mishra, H. Sahoo, Amine functionalized magnetic iron oxide nanoparticles: Synthesis, antibacterial activity and rapid removal of Congo red dye, *J. Mol. Liq.* 282 (2019) 428–440, <https://doi.org/10.1016/j.molliq.2019.03.033>.
- [60] H. Zhu, R. Jiang, J. Li, Y. Fu, S. Jiang, J. Yao, Magnetically recyclable Fe₃O₄/Bi₂S₃ microspheres for effective removal of Congo red dye by simultaneous adsorption and photocatalytic regeneration, *Sep. Purif. Technol.* 179 (2017) 184–193, <https://doi.org/10.1016/j.seppur.2016.12.051>.
- [61] J.K. Sahoo, A. Kumar, J. Rath, T. Mohanty, P. Dash, H. Sahoo, Guar gum-coated iron oxide nanocomposite as an efficient adsorbent for Congo red dye, *Desalin. Water Treat.* 95 (2017) 342–354, <https://doi.org/10.5004/dwt.2017.21572>.
- [62] R. Wo, Q.-L. Li, C. Zhu, Y. Zhang, G.-F. Qiao, K.-y. Lei, P. Du, W. Jiang, Preparation and characterization of functionalized metal-organic frameworks with core/shell magnetic particles (Fe₃O₄@SiO₂@MOFs) for removal of congo red and methylene blue from water solution, *J. Chem. Eng. Data.* 64 (6) (2019) 2455–2463, <https://doi.org/10.1021/acs.jced.8b01251>.
- [63] C. Wang, Y. Le, B. Cheng, Fabrication of porous ZrO₂ hollow sphere and its adsorption performance to Congo red in water, *Ceram. Int.* 40 (7) (2014) 10847–10856, <https://doi.org/10.1016/j.ceramint.2014.03.078>.
- [64] P. Koohi, A. Rahbar-kelishami, H. Shayesteh, Efficient removal of congo red dye using Fe₃O₄/NiO nanocomposite: Synthesis and characterization, *Environ. Technol. Innov.* 23 (2021), <https://doi.org/10.1016/j.eti.2021.101559>.
- [65] M. Akgül, Enhancement of the anionic dye adsorption capacity of clinoptilolite by Fe³⁺-grafting, *J. Hazard. Mater.* 267 (2014) 1–8, <https://doi.org/10.1016/j.jhazmat.2013.12.040>.
- [66] E.C. Nnadozie, P.A. Ajibade, Isotherm, kinetics, thermodynamics studies and effects of carbonization temperature on adsorption of Indigo Carmine (IC) dye using C. odorata biochar, *Chem. Data Collect.* 33 (2021) 100673, <https://doi.org/10.1016/j.cdc.2021.100673>.
- [67] F. Banisheykholeslami, M. Hosseini, G. Najafpour Darzi, Design of PAMAM grafted chitosan dendrimers biosorbent for removal of anionic dyes: adsorption isotherms, kinetics and thermodynamics studies, *Int. J. Biol. Macromol.* 177 (2021) 306–316, <https://doi.org/10.1016/j.ijbiomac.2021.02.118>.
- [68] F.A. Razmi, N. Ngadi, S. Wong, I.M. Inuwa, L.A. Opotu, Kinetics, thermodynamics, isotherm and regeneration analysis of chitosan modified pandan adsorbent, *J. Clean. Prod.* 231 (2019) 98–109, <https://doi.org/10.1016/j.jclepro.2019.05.228>.
- [69] G. Sarojini, S.V. Babu, M. Rajasimman, Adsorptive potential of iron oxide based nanocomposite for the sequestration of congo red from aqueous solution, *Chemosphere.* 287 (2022) 132371, <https://doi.org/10.1016/j.chemosphere.2021.132371>.
- [70] N.A. Ahammad, M.A. Zulkifli, M.A. Ahmad, B.H. Hameed, A.T. Mohd Din, Desorption of chloramphenicol from ordered mesoporous carbon-alginate beads: effects of operating parameters, and isotherm, kinetics, and regeneration studies, *J. Environ. Chem. Eng.* 9 (1) (2021) 105015, <https://doi.org/10.1016/j.jece.2020.105015>.
- [71] A.R.K. Gollakota, V.S. Munagapati, K.P. Shadangi, G.M. Reddy, J.C. Wen, C.M. Shu, Encapsulating toxic Rhodamine 6G dye, and Cr(VI) metal ions from liquid phase using AlPO₄-5 molecular sieves. Preparation, characterization, and adsorption parameters, *J. Mol. Liq.* 336 (2021), <https://doi.org/10.1016/j.molliq.2021.116549>.
- [72] A.R.K. Gollakota, V.S. Munagapati, V. Volli, S. Gautam, J.-C. Wen, C.-M. Shu, Coal bottom ash derived zeolite (SSZ-13) for the sorption of synthetic anion Alizarin Red S (ARS) dye, *J. Hazard. Mater.* 416 (2021) 125925, <https://doi.org/10.1016/j.jhazmat.2021.125925>.